Basal autophagy regulates receptor tyrosine kinase phosphorylation in colorectal cancer cells via an mTORC2-mediated mechanism

Aikaterini Lampada[1,2], James O'Prey[3], Gyorgy Szabadkai[4], Kevin Ryan[3], Daniel Hochhauser[2]* and Paolo Salomoni[1]*

[1]UCL Cancer Institute, Department of Cancer Biology, London, UK
[2]UCL Cancer Institute, Department of Oncology, London, UK
[3]Beatson Institute, Glasgow, UK
[4]Department of Cell and Developmental Biology, Consortium for Mitochondrial Research, UCL, London, UK

*These authors contributed equally to this work

Running Title: Basal autophagy regulates RTK activation

Correspondence:
Paolo Salomoni
UCL Cancer Institute, Department of Cancer Biology, Paul O'Gorman Building
72 Huntley Street, London, WC1E 6DD, UK
Tel: +44-20-7679-0728
E-mail: p.salomoni@ucl.ac.uk

and

Daniel Hochhauser
UCL Cancer Institute, Department of Oncology, Paul O'Gorman Building
72 Huntley Street, London, WC1E 6DD, UK
Tel: +44-20-7679-6006
E-mail: d.hochhauser@ucl.ac.uk

Abstract

The intracellular autophagic degradative pathway can play tumour suppressive or tumour promoting roles depending on the stage of tumour development. Upon starvation or targeting of oncogenic receptor tyrosine kinases (RTKs), autophagy is activated due to inhibition of PI3K/AKT/mTORC1 signalling pathway and promotes survival, suggesting that autophagy is a relevant therapeutic target in these settings. However, the role of autophagy in cancer cells where the PI3K/AKT/mTORC1 pathway is constitutively active remains only partially understood. Here we report a role for PI3K-independent basal autophagy in regulation of RTK activation in colorectal cancer (CRC) cells. *PI3K* and *RAS*-mutant CRC cells display basal autophagy levels despite constitutive mTORC1 signalling, but fail to increase autophagic flux upon RTK inhibition. Inhibition of autophagy via knockdown of ATG7 leads to decreased phosphorylation of several RTKs, in particular c-MET. Internalised c-MET colocalised with LC3-positive vesicles, but inhibition of autophagy did not affect c-MET intracellular localisation. Finally, autophagy inhibition led to a decrease in mTORC2-mediated phosphorylation of AKT and mTORC2 signalling was linked to the defect in c-MET phosphorylation. Overall, our findings reveal a bi-directional relationship between RTKs and autophagy in CRC cells, with implications for our understanding of autophagy role in cancer cell signalling.

Introduction

Macroautophagy (referred to hereafter as autophagy) is a conserved and tightly regulated catabolic self-renewal pathway that helps cells maintain their homeostasis and overcome stress stimuli. Autophagy mediates the degradation of cytoplasmic long-lived proteins and organelles into lysosomes via their previous engulfment into cytoplasmic double membrane vacuoles, called autophagosomes.[1-4] Autophagy is present at basal levels (basal autophagy) in most cells and tissues and functions as a quality control mechanism for both proteins and organelles. Upon stress, such as nutrient/growth factor deprivation or cancer treatment, autophagy is upregulated in the cell providing nutrient and energy precursors to enable survival.[5, 6] The PI3K/AKT/mTORC1 molecular pathway axis has been described as a master negative regulator of autophagy via its ability to control the initiation steps of this catabolic process.[7-11] Apart from regulating autophagosome initiation, mTORC1 has been recently suggested to control later stages of the autophagic process and specifically autophagosome maturation in nutrient-replete conditions.[12] However, it has been suggested that autophagy can be also regulated via mTOR-independent mechanisms.[13-19]

Autophagy has been found to play an important albeit complex role in cancer initiation and progression. It has been suggested to hold a tumour suppressive function during early tumourigenesis,[20-27] whereas it can also sustain cancer progression.[28-36] Increased levels of basal autophagy have been found in a variety of cancer tissues including colorectal cancer (CRC), where autophagy supports tumour growth and confers tumour aggressiveness.[31]

Autophagy is inhibited by oncogenic tyrosine kinases (OncTKs) and receptor tyrosine kinases (RTKs) via activation of the PI3K/AKT/mTORC1 and RAS/MAPK signalling.[37] In this respect, work from our group and others has shown that induction of

autophagy upon pharmacological targeting of OncTKs/RTKs promotes survival. In turn, pharmacological inhibition of autophagy potentiates OncTK/RTK targeted therapy.[2, 28, 38-41] In particular, autophagy has been placed downstream of two RTKs with a known role in cancer, the Epidermal Growth Factor Receptor (EGFR)[17, 19, 42-50] and the Hepatocyte Growth Factor Receptor (HGFR), c-MET.[51] EGFR has been suggested to regulate autophagy either directly[17, 19] or indirectly through its downstream effectors. Both EGFR and c-MET have been proposed to play tumour-promoting roles in CRC.[52-56] Although autophagy acts as a pro-survival mechanism upon nutrient deprivation in CRC,[57] it remains unclear whether its inhibition could potentiate RTK targeted therapy.

Here, we provide insights into the relationship between autophagy and RTK activation in CRC cells. In most CRC cell lines analysed, autophagy is not induced upon RTK inhibition due to constitutive PI3K/AKT signalling. Accordingly, autophagy inhibition does not potentiate RTK targeted therapy, suggesting that concomitant RTK/autophagy targeting would be of limited efficacy in the clinic. Interestingly, CRC cells display detectable basal autophagic flux despite RAS and PI3K activation. Inhibition of basal autophagy affects tyrosine phosphorylation of several RTKs, in particular c-MET. Internalised c-MET colocalised with LC3-positive vesicles, but inhibition of autophagy did not affect c-MET intracellular localisation. The effect on c-MET phosphorylation upon autophagy inhibition is functionally linked to decreased mTORC2 signalling. Overall, our findings suggest a previously unreported function of basal autophagy in the regulation of mTORC2 and RTK activation, with implications for our understanding of the role of autophagy in cancer cell signalling.

Results

Autophagy is not induced upon RTK inhibition due to constitutive PI3K/AKT signalling in CRC cells

Work from our lab and others has shown that autophagy is induced upon pharmacological targeting of OncTKs/RTKs in cancer cells due to inhibition of the PI3K/AKT/mTORC1 pathway and mediates survival.[28, 39, 41, 42, 45, 46] We set out to further investigate the RTK-autophagy pathway in the context of CRC, where RTK signalling is a factor implicated in tumour development and is being targeted clinically. In particular, several agents targeting EGFR and other members of the ErbB family are currently being tested in CRC trials.[55, 56, 58, 59] These include monoclonal antibodies that specifically bind to EGFR extracellular domain and tyrosine kinase inhibitors (TKIs), which target the intracellular tyrosine kinase domain of EGFR.[60, 61] One could hypothesise that autophagy induction could mediate resistance to EGFR therapy, as previously shown in the context of BCR/ABL pharmacologically inhibition.[28] Unlike in CML, activating mutations of *PI3K* and *KRAS* oncogenes are present in a significant proportion of CRC patients and are associated with resistance to EGFR targeted therapy and tumour aggressiveness.[54, 62] Constitutive PI3K signalling should inhibit autophagy via mTORC1 (ref [9]), whereas *KRAS* mutations are predicted to either inhibit (via PI3K/mTORC1) or activate autophagy.[37] As a result, we first investigated whether EGFR targeted therapy could induce autophagy in a panel of CRC cell lines in relation to *KRAS* and *PI3K* mutational status (Supplementary Figure 1a). We confirmed *KRAS* mutational status in isogenic HCT-116, DLD-1 and SW48 cells (Supplementary Figure 1a-b). CaCo2 cells were found to be heterozygous for *KRAS* G12S point mutation and DiFi cells were *KRAS* WT (Supplementary Figure 1a-b). Regarding *PIK3CA* mutational status, CRC cell lines included in the panel were heterozygous for activating *PIK3CA* point mutations with the exception of CaCo2 and DiFi cells that were *PIK3CA* WT

(Supplementary Figure 1a and c). All cell lines were treated with two different Cetuximab concentrations and LC3B levels were detected by immunoblotting. We also included chloroquine (CQ) treatment, as this allowed us to measure autophagic flux.[63] Only DiFi cells were found to induce moderate autophagy levels upon Cetuximab treatment at both concentrations examined (Figure 1a). DLD-1, HCT-116, SW48 both *KRAS* WT and mutant cells as well as CaCo2 cells failed to induce autophagy by Cetuximab treatment at any concentration examined (Figure 1b-e). Similar results were obtained by treating cells with the TKI Gefitinib or RNAi-mediated EGFR downregulation (Supplementary Figure 2a-b). PI3K is a family of lipid kinases, which catalyse the phosphorylation of the 3-hydroxyl group of the inositol ring in phosphatidylinositols (Ptdlns). Class I PI3Ks are downstream effectors of RTKs and they generate phosphatidylinositol 3,4,5 tri-phosphate (PIP3) from phosphatidylinositol 4,5 bi-phosphate (PIP2) that recruits AKT protein kinase and 3-phosphoinositide-dependent kinase 1 (PDK1) to the plasma membrane priming in that manner AKT/mTORC1 pathway activation.[64] Rat sarcoma protein (RAS) is belonging to the large family of small GTPases, which switch constantly from an inactive GDP-bound state to an active GTP-bound state. RAS are activated in response to active RTK signalling and catalyse the activation of RAF protein, which in turn phosphorylates MEK that finally leads to the phosphorylation of ERK1/2 proteins.[65] Additionally, RAS can directly activate PI3K and in that manner regulate AKT/mTORC1 pathway.[64]

As EGFR inhibition failed to induce autophagy in most CRC cell lines analysed, we hypothesised that treatment with the lysosomotropic autophagy inhibitor CQ would not affect sensitivity of CRC cells to Cetuximab with the potential exception of DiFi cells, which induced autophagy following EGFR targeted therapy**.** Indeed, CQ treatment did not sensitise cells carrying *PI3K* and/or *KRAS* mutations to Cetuximab treatment (Supplementary Figure 3a-d). Of note, autophagy inhibition by CQ was

found to only marginally potentiate Cetuximab treatment in DiFi cells (Supplementary Figure 3e). CQ treatment alone did not affect CRC cell growth in the majority of the cell lines examined (Supplementary Figure 3a-d).

As constitutive PI3K signalling is expected to lead to mTORC1-dependent inhibition of autophagy, we next examined the activation status of the PI3K/AKT pathway upon Cetuximab treatment. We observed that the phosphorylation of S473 residue of AKT was not downregulated upon Cetuximab treatment in HCT-116, DLD-1 and CaCo2 cells (Supplementary Figure 4b-d). More specifically, AKT phosphorylation levels were increased upon Cetuximab treatment in DLD-1 and HCT-116 cells, whereas they were reduced in DiFi cells (Supplementary Figure 4a). Overall, these data suggest a correlation between KRAS and/or PI3K/AKT activation and failure to induce autophagy in CRC cells. In summary, resistance to induce autophagy upon EGFR inhibition correlated with *PI3K* mutational status in CRC cell lines, with the exception of CaCo2 cells.

In order to establish a link between AKT activation levels and autophagy induction upon Cetuximab treatment, we generated DiFi cells stably expressing myristoylated-AKT (LXSN_myrAKT). myrAKT protein is localised to the plasma membrane and remains constitutively active.[18, 66] As expected, cells overexpressing myrAKT displayed higher pAKT levels at both steady state and upon Cetuximab treatment (Supplementary Figure 4e). Increased activation levels of AKT in LXSN_myrAKT DiFi cells resulted in lower autophagy induction levels upon Cetuximab treatment when compared with control DiFi cells (Supplementary Figure 4e), implying a functional link between AKT activation status and autophagy induction in CRC cells upon Cetuximab treatment.

We next tested whether the use of the AKT vIII inhibitor could de-repress autophagy in *PIK3CA*-mutated cells following Cetuximab treatment. We found that AKT vIII

inhibitor alone or in combination with Cetuximab was able to downregulate pAKT levels compared to untreated or Cetuximab-only treated E545K and D549N *PIK3CA* mutant DLD-1 *KRAS* WT and mutant cells (Supplementary Figure 4f). Critically, in the conditions where pAKT levels were abolished, autophagy was induced upon AKT vIII inhibitor treatment alone or in combination with Cetuximab.

Overall, our findings indicate that *PI3K* and *KRAS* mutations make CRC cells refractory to autophagy induction upon RTK inhibition due to constitutive activation of the PI3K/AKT pathway.

Inhibition of PI3K-independent basal autophagic flux negatively affects RTK phosphorylation in CRC cells

We noted that CRC cells were found to have basal levels of autophagy in unstimulated conditions (Figure 1f-i). In particular, the basal autophagic flux was independent of *KRAS* and *PIK3CA* mutational status, as both *KRAS* WT and *KRAS* mutant isogenic cell lines as well as *PIK3CA* WT (CaCo2 and DiFi) and *PIK3CA* mutant (HCT-116 and DLD-1) CRC cell lines displayed increased LC3-II/LC3-I ratio following CQ treatment (Figure 1f-i). We hypothesised that autophagy might not play a significant degradative role in CRC cells under basal conditions. In this respect, levels of p62, an autophagy adaptor involved in targeting of polyubiquitinated proteins and organelles for lysosomal degradation through binding LC3 on phagophore membranes, were examined. Inhibition of autophagic flux results in accumulation of p62 levels.[67] However, in CRC cells p62 levels were not significantly affected by either CQ or inhibition of autophagy via a doxycycline (Dox)-inducible shRNA against ATG7, an essential autophagy gene (Supplementary Figure 5a-c). Based on these findings, we thought to investigate whether basal autophagy could affect cell signalling in fed-conditions as previously reported.[68, 69] Specifically, we set out to investigate whether autophagy suppression could impact on RTK activation,

given the key role of RTKs in CRC pathogenesis. To this end, we utilised a phospho-RTK array to evaluate the phosphorylation of 49 different RTKs. Activated *KRAS* G13D isogenic cell lines were also included in this examination in order to assess whether the presence of oncogenic *KRAS* affects autophagy-dependent RTK regulation. Interestingly, phosphorylation of eight different RTKs was decreased upon autophagy suppression in HCT-116 *KRAS* WT cells (Figure 2a-b). In particular, autophagy-compromised cells displayed a decrease in phosphorylation levels of the highly activated RTKs: i) c-MET (35%), member of HGFR RTK family; ii) Dtk (35%), member of AXL RTK family; iii) c-Ret (60%), member of the RET RTK family and iv) RYK (40%). In the same cells, RTKs with lower phosphorylation levels were also affected, such as TrkC (90%), EphA1 (46%), EphA2 (30%) and EphB2 (60%). Overall, autophagy inhibition led to reduced phosphorylation of 8 out of 49 RTKs included in the array. RTK phosphorylation was also affected in autophagy-suppressed *KRAS* G13D HCT-116 cells: c-Ret (60%), c-Met (47%), MSP receptor (42%), EphA10 (38%), Dtk (30%), Insulin Receptor (26%), IGF-I receptor (22%), Axl (17%) and ROR2 (15%) (Figure 2a and c). In contrast to HCT-116 *KRAS* WT cells, autophagy suppression resulted in upregulated phosphorylation of TrkC RTK (~70%) in the presence of the *KRAS* G13D mutation (Figure 2a-c). To exclude a cell type-specific effect of autophagy suppression, DLD-1 *KRAS* WT and G13D cells were also examined for RTK activation levels upon autophagy suppression. In accordance with the reduced RTK-phosphorylation phenotype observed in HCT-116 autophagy-compromised cells, both DLD-1 *KRAS* WT and G13D autophagy-compromised cells displayed a decrease in phosphorylation of several RTKs (Supplementary Figure 6a-c).

In conclusion, autophagy suppression reduced phosphorylation of several RTKs in CRC cells, in most cases independently of *KRAS* mutational status.

Inhibition of basal autophagy downregulates c-MET phosphorylation

We decided to focus on c-MET since it has been proposed to play an oncogenic role in CRC[52] and it has been implicated in the development of primary and acquired resistance of mCRC cells and patients to EGFR-targeted therapy.[53, 54] In line with the phospho-RTK array results, immunoprecipitated total c-MET was found to be less phosphorylated in autophagy-compromised cells compared to autophagy-proficient HCT-116 *KRAS* WT cells (Figure 3a). In contrast, phosphorylation levels of both IGF-I R and EGFR were not affected following basal autophagy suppression, confirming results of the phospho-RTK array (Supplementary Figure 7a-b). Of note, total tyrosine-phosphorylation levels were not altered upon autophagy suppression (Figure 3a and Supplementary Figure 7a-b). We further confirmed that basal autophagy suppression reduces phosphorylation of c-MET using a phospho-specific c-MET antibody. The ratio between phosphorylated c-MET and total c-MET was decreased in total cell lysates from autophagy-compromised HCT-116 *KRAS* WT and G13D cells by approximately 40% and 30%, respectively (Figure 3b). Phosphorylation of c-MET was consistently reduced in HCT-116 cells where ATG7 was knocked out using CRISPR/Cas9 technology (Figure 3c) and in autophagy-compromised CaCo2 cells (Figure 3d). Total c-MET levels were unaltered in autophagy-compromised and autophagy-deficient cells (Figure 3b-d). Although autocrine c-MET activation in cancer has been previously described,[70] we failed to detect any differences in HGF expression in lysates from ATG7 and LC3B knockdown cells (Supplementary Figure 7c).

c-MET colocalises with LC3B positive intracellular structures but autophagy suppression does not alter c-MET localisation

Evidence from the literature suggests that RTKs colocalise with autophagic structures, thus suggesting that autophagy may regulate c-MET by controlling its internalization or intracellular function.[71, 72] To explore this, HCT-116 cells were

examined for endogenous c-MET and LC3B protein localisation using confocal microscopy. To increase the chances of detecting autophagosomes, we added CQ, which prevents their fusion with lysosomes and subsequent degradation.[63] After CQ treatment c-MET was observed in punctate intracellular structures around the nucleus that colocalised with LC3B only in autophagy-proficient conditions (Figure 4a). To determine whether this colocalisation pattern applied to another RTK, localisation of EGFR was examined upon CQ treatment in HCT-116 *KRAS* WT cells. It was observed that in contrast to c-MET, EGFR did not accumulate in perinuclear areas upon CQ treatment and no colocalisation with LC3B was observed (Figure 4b).

We additionally investigated whether basal autophagy suppression is affecting localisation of c-MET and in that manner c-MET phosphorylation. To this end, we treated autophagy-proficient and -compromised HCT-116 cells with 10μM CQ and monitored c-MET localisation using confocal microscopy for endogenous c-MET. It was found that basal autophagy suppression did not change intracellular c-MET accumulation (Figure 4c).

Basal autophagy-mediated regulation of c-MET phosphorylation is linked to mTORC2

We then investigated whether reduced RTK phosphorylation was associated with alterations of main signalling pathways. In this respect, we noted that upon doxycycline (Dox) treatment, CRC cells displayed reduced mTORC2-mediated phosphorylation of AKT (pAKT S473) relative to levels of total AKT (Figure 5a-c). Specifically, HCT-116 *KRAS* WT, DLD-1 *KRAS* WT and CaCo2 autophagy-compromised cells displayed approximately 25%, 35% and 30% downregulation of pAKT S473, respectively. pAKT downregulation was more evident in the presence of *KRAS* G13D in HCT-116 and DLD-1 cells (35% and 65%, respectively; Figure 5a-c). Notably, pAKT S473 downregulation was confirmed in ATG7-deficient HCT-116 cells (Figure 5g). Reduced pAKT S473 was not associated with decreased

phosphorylation levels of the mTORC1 downstream target, S6 ribosomal protein (Figure 5d-f). Specifically, HCT-116 and DLD-1 *KRAS* WT autophagy-compromised cells showed increased rather than decreased S6 phosphorylation (~40% and ~15% respectively) when compared to their autophagy-proficient controls. In HCT-116 and DLD-1 *KRAS* G13D cells, pS6 ribosomal protein S240/244 levels remained unaffected upon autophagy downregulation. CaCo2 autophagy-compromised cells displayed a reduction in pS6 ribosomal protein S240/244 levels, albeit not statistically significant. Sustained activation of mTORC1 following autophagy suppression was further confirmed in ATG7 knockout HCT-116 cells (Figure 5h). Together, these data suggest that autophagy inhibition affects mTORC2 but not mTORC1 activity.

Since inhibition of mTORC2-dependent AKT phosphorylation occurred also in cells where PI3K signalling is constitutively active (via *PI3K* activating mutations), we speculated that these signalling changes are upstream rather downstream the defect in RTK phosphorylation. Previous reports have shown that RTK signalling activates mTORC2 (ref [73]) and vice versa mTORC2 promotes RTK activation.[74] As a result, we investigated whether inhibition of mTORC2 could affect c-MET phosphorylation. Autophagy-proficient and-compromised cells were treated with 2nM of Torin2 inhibitor that targets mTOR kinase activity and results in both mTORC1 and mTORC2 inhibition. Torin2 treatment downregulated mTORC2-mediated phosphorylation of AKT at S473 residue as well as phosphorylation of S6 ribosomal protein downstream of mTORC1 in both autophagy-proficient and autophagy-compromised cells. Interestingly, Torin2 treatment decreased c-MET phosphorylation in autophagy-proficient cells to the similar extent to suppression of autophagy. Finally, Torin2 treatment did not further reduce c-MET phosphorylation in autophagy-compromised conditions (Figure 6a).

In an attempt to further confirm that basal autophagy-dependent regulation of mTORC2 controls c-MET phosphorylation, we investigated whether induction of

mTORC2 kinase activity could increase c-MET phosphorylation. To this end, we employed the mTORC1 inhibitor Rapamycin, which is known to upregulate mTORC2 activity through inhibition of a mTORC1-mediated negative feedback loop.[75-77] Autophagy-proficient and-deficient HCT-116 cells were treated with Rapamycin and analysed at different time points. Rapamycin downregulated mTORC1 activity and led to increased mTORC2-mediated phosphorylation of AKT at S473. Notably, rapamycin-mediated mTORC2 upregulation resulted in accelerated phosphorylation of c-MET in autophagy-proficient cells but not in autophagy-deficient cells. (Figure 6b).

Collectively, our data suggest that basal autophagy regulates RTK activation at least in part in an mTORC2-dependent manner.

Discussion

Autophagy plays a complex role in cancer, which still remains not fully understood. It has been proposed by us and others that in established tumours autophagy plays a pro-survival role,[28, 39, 41, 42, 45, 46, 57] in particular upon starvation or downstream inhibition of oncogenic kinase signalling, both of which result in inhibition of the main autophagy inhibitor, the PI3K/AKT/mTORC1 pathway. However, little is known on the role of autophagy and autophagy-like pathways in the presence of active PI3K/AKT/mTORC1 signalling in cancer cells, due to mutations in either PI3K or RAS pathway. As a model, we chose CRC, since PI3K and RAS pathways are often constitutively active, and RTK signalling is a factor implicated in cancer development and is being targeted clinically.[55, 56, 58, 59] On one hand, we show that autophagy is not a relevant target for pharmacological intervention upon RTK inhibition when the PI3K/AKT pathway is constitutively active. On the other hand, we have disclosed a novel pathway, whereby *KRAS* and *PI3K*-independent basal autophagy positively regulates RTK activation through mTORC2 signalling.

EGFR targeted therapy has been characterised as a potent autophagy-inducing stimulus in cancer cells[17, 19, 42, 44, 45, 48-50] via inhibition of the PI3K.[42, 45, 46] However, we show here that constitutive activation of the PI3K/AKT pathway, downstream *KRAS* and/or *PI3K* activating mutations, blocks autophagy induction following EGFR inhibition in CRC cells. Our findings suggest that concomitant targeting of EGFR and autophagy in clinical settings would not be beneficial in *KRAS* or *PI3K*-mutated CRC patients.

Interestingly, we found that all CRC cell lines utilised in this work exhibit basal autophagic flux irrespective of their *PI3K* or *KRAS* mutational status. Although earlier studies have suggested that autophagy can be regulated in an mTORC1-independent manner,[13-19] the role of basal autophagy in cancer remains elusive. We hypothesised that basal autophagy would not play a major degradative role in fed-conditions, whereas it could affect cell signalling as previously reported.[68, 69] Specifically, we set out to investigate whether autophagy suppression could impact on RTK activation. To this end, we analysed RTK tyrosine phosphorylation upon knockdown of the essential autophagy gene ATG7. Interestingly, we found that basal autophagy suppression reduces RTK phosphorylation, including c-MET, c-RET and Dtk in CRC cells, in most cases independently of *KRAS* mutational status. We decided to focus on c-MET, since it has been proposed to play an oncogenic role in CRC[52] and it has been implicated in the development of primary and acquired resistance of mCRC cells and patients to EGFR-targeted therapy.[53, 54] Levels of total c-MET remained stable following basal autophagy suppression ruling out the possibility that the decrease in phosphorylation levels of c-MET is caused by decreased c-MET expression and/or degradation. Additionally, our findings suggest that basal autophagy-mediated regulation of RTK phosphorylation is not attributed to a general metabolic control of tyrosine-phosphorylation levels since the latter were not altered upon basal autophagy suppression and furthermore EGFR and IGF-IR β

phosphorylation was not altered following autophagy suppression. Therefore, we suggested that an unconventional non-catabolic function of basal autophagy is responsible for the regulation of RTK phosphorylation and c-MET specifically.

The function of the autophagosome as a cell-signalling regulator in a non-catabolic manner has only recently been reported in the literature.[68, 69] In this respect, we observed that basal autophagy suppression decreased mTORC2-mediated regulation of AKT in a non-degradative manner but did not alter mTORC1 activity, thus ruling out that autophagy-dependent regulation of mTORC2 is dependent on the previously reported mTORC1 negative feedback loop.[78] The decrease in mTORC2 signalling occurred in cells where the PI3K pathway is constitutively active due to *PI3K* activating mutations, suggesting that it was not caused by inhibition of RTK phosphorylation. Therefore, we asked whether reduced mTORC2 signalling responsible for the defect in RTK phosphorylation? Indeed, pharmacological inhibition of mTORC1/2 led to decreased c-MET phosphorylation in autophagy-proficient but not autophagy-suppressed cells. Vice versa, rapamycin, which activates mTORC2, led to increased c-MET phosphorylation. Although we cannot exclude that decreased mTORC2 signalling in autophagy-impaired cells is in part due to inhibition of RTK signalling, our data suggest that autophagy positively mediates RTK phosphorylation via regulation of mTORC2 signalling. In this respect, mTORC2 activity has been previously described to directly regulate IGF-IR and IR phosphorylation in an mTOR kinase activity-dependent manner.[74] Since there was no tight correlation between increased levels of p-c-MET and pAKT S473 upon rapamycin treatment (3 and 6 hour timepoints), autophagy may directly regulate c-MET activation through mTORC2, potentially without a substantial involvement of AKT.

One outstanding question is how autophagy regulates AKT and c-MET phosphorylation. We hypothesised that internalised c-MET could interact with

autophagy vesicles. Indeed, our findings show that c-MET partially colocalises with LC3B-positive structures intracellularly, whereas no colocalisation was observed with EGFR, which is not affected by autophagy inhibition in the phospho-RTK arrays. Interestingly, intracellular localisation of c-MET was not affected by autophagy suppression, suggesting that autophagic or autophagic-like vesicles do not regulate RTK internalisation but may represent signalling platforms regulating RTK phosphorylation. In this respect, AKT activity regulation through mTORC2 in intracellular compartments such as lysosomes has been previously described.[79] Furthermore, autophagy has been previously shown to affect ERK and AKT signalling.[68, 69]

In overall, this work establishes an unconventional role of basal autophagy in regulation of RTK activation and suggest a bidirectional relationship between autophagy and RTK signalling: on one hand RTKs inhibit autophagy via mTORC1, while on the other hand autophagy positively modulate RTK signalling via mTORC2 activation. Further work is needed to fully dissect the mechanisms by which autophagy controls RTK signalling in cancer cells.

Materials and Methods

Chemical compounds and drugs

All chemical compounds and drugs were dissolved in an initial stock concentration and then in cell culture media to reach the final working concentration. Sterile conditions were followed throughout the preparation of all reagents. Fresh aliquots were used for each independent experiment. Chloroquine diphosphate salt (CQ) [#C6628, Sigma (Dorset, UK)] was dissolved in sterile Phosphate Buffered Saline (PBS) and was used at a concentration of 10 μM. Doxycycline hyclate (Dox) powder (#D9891, Sigma) was resuspended into sterile H_2O and was used at the optimal working concentration of each CRC cell line (10 ng/ml for HCT-116; 100 ng/ml for

DLD-1 and CaCo2 cells). Dox was used for stimulation of shRNA expression in the pLKO-Tet-On inducible CRC cell lines. Clinical-grade Cetuximab and Gefitinib were used. Cetuximab (5 mg/ml) was obtained from Merck Serono (Darmstadt, Germany). All following drugs were dissolved in dimethyl sulfoxide (DMSO) (#D2650, Sigma). Clinical-grade Gefitinib [Iressa®; AstraZeneca (London, UK)] was used at a concentration of 1 μM and the AKT inhibitor vIII [#124018, Calbiochem®, Merck Millipore (Darmstadt, Germany)] was used in the indicated concentrations. Torin2 (#475992, Calbiochem) was used at a concentration of 2 nM. Rapamycin [#R5000, LC Laboratories (Woburn, MA, USA)] was used in a concentration of 10 nM. In all experiments wherein cells were treated with compounds diluted in DMSO, the corresponding untreated conditions were treated with equal concentrations of DMSO.

Plasmids

A Dox-inducible system was used to knockdown ATG7 protein in CRC cells by using the Tet-pLKO-puro vector [Addgene plasmid #21915, Addgene (Cambridge, MA, USA)], established by Dmitri Wiederschain lab.[80] The CRISPR/Cas9 system was used to delete *ATG7* by using the lentiCRISPR vector (Addgene plasmid #52961), established by the Zhang lab.[81] pLXSN and pLXSN_myrAKT plasmids were kindly provided by Dr Pablo Rodriguez-Viciana (University College London, UK).

Antibodies

Antibodies against human LC3B [1/1000; #2775, Cell Signaling Technology (Leiden, The Netherlands)], ATG7 (1/500; #2631, Cell Signaling Technology), β-actin (1/5000; #A5441, Sigma) and HGF [1/1000; #ab83760; Abcam (Cambridge, UK)] were diluted in 5% milk (w/v) 1X PBS - 0.1% Tween-20 (Sigma) in the corresponding concentration and used for immunoblotting. Antibodies against human pAKT S473 (1/1000; #4060, Cell Signaling Technology), total AKT (1/1000; #9272, Cell Signaling Technology), total AKT (1/1000; #2920, Cell Signaling Technology), Calnexin (1/1000; #2433, Cell Signaling Technology), pS6 ribosomal protein S240/244

(1/1000; #2215, Cell Signaling Technology), total S6 ribosomal protein (1/500; #2317, Cell Signaling Technology), total IGF-IR beta (1/1000; #3027, Cell Signaling Technology), total EGFR (1/500; #2232, Cell Signaling Technology), p-c-MET Y1234/1235 (1/500; #3077, Cell Signaling Technology), total c-MET (1/1000; #8198, Cell Signaling Technology) and phosphotyrosine clone 4G10 (1/500-1/1000; #05321, Merck Millipore) were diluted in 5% BSA (w/v) 1X TBS – 0.1% Tween-20 (Sigma) in the corresponding concentration and used for immunoblotting. For immunoprecipitation studies the antibodies against human total c-MET (#8198, Cell Cell Signaling Technology), total EGFR (#4267, Cell Signaling Technology), total IGF-IR beta (#3027, Cell Signaling Technology) and normal IgG (#2729, Cell Signaling Technology) were used. For immunofluorescence experiments the antibodies against human LC3B [1/50; #0231-100/LC3-5F10, nanoTools Antikörpertechnik GmbH & Co. KG (Teningen, Germany)], total c-MET (1/150; #8198, Cell Signaling Technology) and total EGFR (1/50; #4267, Cell Signaling Technology) were used. Secondary antibodies used for immunoblotting were goat anti-rabbit IgG DyLight 800 [1/5000; #35571, Thermo Fisher Scientific (Waltham, MA, USA)], goat anti-mouse IgG DyLight 680 (1/5000; #35518, Thermo Fisher Scientific), ECL anti-rabbit IgG [1/5000; #NA934V, GE Healthcare UK Limited (Hatfield, UK)] and ECL anti-mouse IgG (1/5000; #NA931V, GE Healthcare UK Limited). Anti-rabbit IgG Alexa Fluor 555 (1/1000; #A31572, Invitrogen-Thermo Fisher Scientific) and anti-mouse IgG Alexa Fluor 647 (1/1000; #A31571, Invitrogen-Thermo Fisher Scientific) secondary antibodies were used for immunofluorescence experiments.

Cell culture

HCT-116 and DLD-1 *KRAS* WT and G13D isogenic cell lines were kindly provided by Prof. Bert Vogelstein (Johns Hopkins University, USA). SW48 *KRAS* isogenic cell lines were purchased from the Horizon Discovery (Cambridge, UK). DiFi cells were kindly provided by Prof. Alberto Bardelli (University of Torino, Torino, Italy). Cells

were cultured in tissue culture dishes at 37^{o}C in a humidified atmosphere of 5% CO_2. HCT-116, DLD-1 and SW48 cells were maintained in McCoy's 5A medium containing 2 mM L-Glutamine. CaCo2 cells were maintained in Minimum Essential Medium (MEM) medium containing 2 mM L-Glutamine. DiFi cells were maintained in Ham's F12 Nutrient mixture medium containing 1 mM L-Glutamine. HCT-116 CRISPR Ctrl and ATG7 cells as well as the human embryonic kidney cell line HEK-293T were maintained in Dulbecco's Modified Eagle's Medium (DMEM) supplemented with 4.5 g/L D-Glucose and Sodium Pyruvate. The human embryonic kidney cell line, Phoenix A was maintained in Iscove's Modified Dulbecco's Medium (IMDM) containing 4.5 g/L D-Glucose and Sodium Pyruvate. All cell culture media were supplemented with 10% Fetal Bovine Serum (FBS, Thermo Fisher Scientific), and 1% Penicillin/Streptomycin (Gibco-Thermo Fisher Scientific). All inducible pLKO-Tet-On shRNA-expressing (shEGFP, shATG7-E8 and -G7) stable cell lines were maintained in corresponding medium supplemented with 10% Tet-Free Certified FBS (#16000-044, Lot number 1221032, Thermo Fisher Scientific). Cell number counting and cell viability examination was conducted using the Vi-Cell XR machine and software (Beckman Coulter, Indianapolis, IN, USA).

Transient transfection for small interfering RNAs (siRNAs) delivery

Two different transfection reagents were used for the delivery of EGFR and LC3B siRNAs to CRC cell lines. SMARTpool: ON-TARGETplus EGFR siRNA (#L-003114-00, GE Healthcare Dharmacon Inc, UK) and siRNA negative control (Scramble, GE Healthcare Dharmacon Inc, UK) were used in a concentration of 25 nM using DharmaFECT reagent 1 (#T-2001-02, GE Healthcare Dharmacon Inc, UK) in HCT-116 cell line. Silencer select LC3B siRNA (#s37749 and #s224886, Thermo Fisher Scientific) and negative control (Scramble, #4390843, Thermo Fisher Scientific) were used in a concentration of 10 nM using Lipofectamine RNAiMAX reagent (#13778075, Thermo Fisher Scientific) in HCT-116 cells. Forward transfection

protocol was followed with both transfection reagents according to the protocol of each manufacturer. Cells were harvested 48 hours post-transfection by scraping and protein knock down was assessed using immunoblotting.

Virus particle production

The calcium phosphate transfection method was used to generate lenti- and retro-virus particles by transfecting HEK 293T and Phoenix A cells with the corresponding plasmids, respectively. For pLKO-Tet-On shEGFP and shATG7 E8 or G7 -lentivirus particle production, 6 x 10^6 HEK 293T cells were plated in 15 cm dishes containing 20 ml complete DMEM medium and were let to adhere overnight at 37^o C. The following day, a triple co-transfection of HEK 293T cells with lentivirus packaging/envelope vectors and desired plasmid DNA was performed [7.2 µg of pCMV-VSV-G; 15.6 µg pCMV-HIV-1; 24 µg of shRNA encoding lentivirus vector (pLKO-Tet-On shEGFP or shATG7 E8 / G7)]. For CRISPR/Cas9 -Ctrl or -ATG7 gRNAs -lentivirus particle production, 1.5 x 10^6 HEK 293T cells were plated in 10 cm dishes containing 10 ml complete DMEM medium and were let to adhere overnight at 37^o C. The following day, a triple co-transfection of HEK 293T cells with lentivirus packaging/envelope vectors and desired plasmid DNA was performed [7.5 µg of psPAX2; 4 µg of VSV-G; 10 µg of lentiCRISPR vectors encoding (Cas9 and Ctrl or ATG7 gRNAs)]. DNA-mixture was diluted in sterile nuclease free H_2O containing 10% (v/v) 2.5 M calcium chloride to a final volume of 1 ml. For retrovirus particle production, 2.5 x 10^6 Phoenix A cells were plated in 10 cm dishes containing 10 ml complete IMDM medium and were let to adhere overnight at 37^{o}C. The following day, Phoenix A cells were co-transfected with 1.2 µg SARAIII retrovirus packaging vector and 20 µg desired plasmid DNA (pLXSN or pLXSN_myrAKT). DNA was diluted in sterile nuclease free H_2O containing 25% (v/v) 1 M calcium chloride to a final volume of 1 ml.

For both lenti- and retro- virus production, the DNA-calcium chloride mixture was thoroughly mixed and allowed to equilibrate at room temperature for 30 min. 37^{o}C pre-warmed 2X HEPES pH 7.05 buffer [280 mM NaCl; 10 mM KCl; 1.5 mM Na_2HPO_4; 12 mM D(+)-Glucose Monohydrate; 50 mM HEPES] was added to the DNA-calcium chloride solution in a ratio 1:1 and the mixture was thoroughly mixed for 1 min. DNA-calcium chloride-HEPES mixture was added dropwise to each 15 cm/10 cm dish containing HEK 293T cells or 10 cm dish containing Phoenix A cells. Transfection medium was replaced with normal culture medium after 8 hours. Transfected HEK 293T cells and transfected Phoenix A cells were let to incubate for additional 48 and 36 hours, respectively, when supernatants containing viral particles collected.

Viral particles concentration by polyethylene glycol (PEG) precipitation was performed for pLKO-Tet-On shEGFP and shATG7 E8 or G7 -lentivirus particles and pLXSN_myrAKT/pLXSN retrovirus particles. Briefly, supernatants containing lenti- or retro- virus particles were centrifuged at 3000 g for 15 min to eliminate cells and cellular debris. Further cellular debris elimination was achieved by 0.45 μm PVDF filtration of the supernatant. 5X PEG pH 7.2 (50 mM PEG; 0.41 M NaCl; 0.2% Tris 1 M, pH 7.5) solution was added to the supernatant containing the viral particles in a volume ratio 1:4 to concentrate the virus particles. Solution was refrigerated at 4^{o}C overnight. The next day the concentrated virus particles were pelleted down through centrifugation at 1500 g for 30 min and PEG containing medium was discarded. Virus particle pellets were resuspended in sterile cold PBS in a volume ratio 50:1 and were aliquoted and stored at -80^{o} C. Fresh concentrated virus particles aliquots were used in each independent viral transduction experiment. Tittering of virus was performed using antibiotic selection, as was previously described.[80, 82]

For CRISPR/Cas9 -Ctrl or -ATG7 gRNAs -lentivirus particle production, lentivirus-containing supernatant from HEK 293T cells was collected 48 and 72 hours after

transfection and filtered through a 0.45 μm PTFE filter membrane. Lentivirus-containing supernatant was added fresh to the target cells.

Generation of autophagy-compromised/-deficient and myristoylated AKT-expressing CRC cell lines

Viral transduction was used to generate stable inducible-expressing pLKO-Tet-On shRNA autophagy-proficient (shEGFP) and -compromised (shATG7 E8/G7) CRC cell lines, autophagy-proficient (CRISPR Ctrl) and -deficient (CRISPR ATG7) HCT-116 cells as well as myristoylated AKT-expressing (pLXSN_myrAKT) and control (pLXSN) DiFi cells.

For pLKO-Tet-On shRNA and pLXSN -expressing CRC cell lines, 1.0 x 10^5 cells were plated in 6-well plates and let to incubate overnight at 37^o C. Cells were transduced with the appropriate volume of the corresponding concentrated virus based on virus tittering at an MOI of 10 in media containing 5 μg/ml polybrene. 24 hours later, virus-containing medium was replaced by fresh complete medium and target cell lines were let to incubate for additional 24 hours. For CRISPR HCT-116 cells, 0.7 x 10^6 cells were plated in 10 cm dishes and let to incubate overnight at 37^o C. Cells were transduced with the lentivirus-containing supernatant (supernatant-48 hours after transfection) from HEK 293T cells supplemented with polybrene and let to incubate for 24 hours. The following day, fresh lentivirus-containing supernatant (supernatant-72 hours after transfection) from HEK 293T cells was added to HCT-116 target cells for additional 24 hours.

48 hours after viral transduction, antibiotic selection of transduced cell populations was performed using puromycin selection for pLKO-Tet-On-shRNA or CRISPR/Cas9 expressing cells (0.5 μg/ml for HCT-116, 3 μg/ml for DLD-1 and 1.5 μg/ml for CaCo2 cells) and neomycin selection for LXSN_myrAKT (750 μg/ml for DiFi cells) and control cells. Antibiotic-containing medium was replaced every two days for at least a week in order to generate stable cell lines. All experiments were conducted in the

absence of either puromycin or neomycin selection. The inducible downregulation of ATG7 protein was performed in the presence of Dox (10 ng/ml for HCT-116; 100 ng/ml for DLD-1 and CaCo2 cells) for 5 days.

Total cell protein extraction

2.5 - 4 x 10^5 of CRC cells (depending on each CRC cell line) were plated in 6 cm tissue culture dishes and let to adhere for approximately 48 hours at 37^o C until approximately 70% of confluence was reached. Drug treatment was applied under sterile conditions for the indicated incubation time and total cell protein extraction followed. Cell culture medium was removed and adhered cells were washed once with 1X PBS. 100 - 150 µl of RIPA Lysis Buffer [20 mM Tris pH 7.4; 150 mM NaCl; 1 mM EDTA pH 8; 1 mM EGTA pH 8; 0.5% (w/v) Sodium Deoxycholate; 0.1% (v/v) sodium dodecyl sulfate (SDS); 1% (v/v) Nonidet P-40] or Non-Denaturing Lysis Buffer [20 mM Tris pH 7.4; 137 mM NaCl; 2 mM EDTA pH 8; 1% (v/v) Nonidet P-40] supplemented with protease inhibitors [10 µg/ml of each Pepstatin A (#P5318, Sigma), Aprotinin (#A6279, Sigma) and Leupeptin (#L8511, Sigma) or 1X of the protease inhibitor cocktail (#11697498001; Roche, Basel Switzerland)] and phosphatase inhibitors [1 mM Na_3VO_4 (#S6508, Sigma); 50mM NaF (#201154, Sigma)] was added to the cells on ice. Cell scraping was used to harvest cells from the culture dishes and cell lysates were transferred to microcentrifuge tubes. Cell lysates were incubated on ice for 30 min and then centrifuged at 13200 rpm for 15 min at 4^o C. Supernatants containing total cell protein extracts were transferred to new microcentrifuge tubes and kept on ice as long as the total cell protein concentration of extracts was quantified. For determination of total cell protein concentration, the BCA protein assay kit (#23227, Thermo Fisher Scientific) or Bradford assay [#500-0006, BioRad (Hertfordshire, UK)] were used according to instructions of the manufacturer. Following total cell protein concentration quantification, 5X protein loading buffer [10% (w/v) SDS; 50% (w/v) glycerol; 0.125%

(w/v) bromophenol blue; 250 mM Tris pH 6.8; 2 mM 2-mercaptoethanol] was added to cell lysates in a ratio 1:4 in order to yield a final concentration of 1X protein loading buffer to the cell extracts. Total cell extracts were boiled at 95^{o} C for 5 min.

Immunoblotting

Equal concentration of total cell extracts (30 - 50 µg) were separated in 8%, 10%, 15% SDS-polyacrylamide gel electrophoresis (SDS-PAGE) or Criterion™ TGX Stain-Free™ Precast Gels (BioRad) as required and transferred for $2^{1/2}$ hours onto nitrocellulose membrane in a wet blotter. 1X Running Buffer [0.186M Glycine; 0.02 M Trisma Base; 0.15% (v/v) SDS] was used for protein electrophoresis and 1X Transfer Buffer [0.186M Glycine; 0.02 M Trisma Base; 20% (v/v) Methanol] was used for protein transfer. Efficiency of protein transfer onto nitrocellulose membranes was examined by shortly incubating membranes in Ponceau S (Sigma) solution that reversibly removed by 1X PBS – 0.1% Tween-20 or 1X TBS – 0.1% Tween-20 washes. Nitrocellulose membranes were blocked in 5% BSA (w/v) 1X TBS – 0.1% Tween-20 for phosphorylated studies and in 5% milk (w/v) 1X PBS – 0.1% Tween-20 for all other studies with 1 hour incubation time. Immunodetection performed by incubating membranes with primary antibody overnight at 4^{o}C and with the corresponding secondary antibody diluted in 5% milk (w/v) 1X PBS – 0.1% Tween-20 for 1 hour. Protein expression was detected on medical X-Ray films using the Enhanced Chemiluminescence System (ECL) when HRP-conjugated secondary antibodies used. The Odyssey imaging System scanner (LI-COR Biotechnology - UK Ltd, Cambridge, UK) was used for detection of protein expression when fluorescent dye-conjugated secondary antibodies were used. LI-COR Odyssey software or Fiji (Image-J, NIH, MD, USA) software was used for densitometric analysis of protein bands detected either via LI-COR Odyssey Imaging System scanner or ECL, respectively.

Immunoprecipitation (IP)

Lyophilised protein A Sepharose beads (#71-7090-00AF, GE Healthcare UK Limited) were hydrated in distilled H_2O based on the instructions of the manufacturer and followed coupling of the protein A Sepharose beads with the antibodies used in IP studies. Briefly, the Sepharose protein A slurry was gently mixed by vortexing and 10 µl of beads were washed twice with non-denaturing lysis buffer by intermediate centrifugations of 20 sec at 13200 rpm. Followed coupling of beads with the required volume of antibody in 300 µl of non-denaturing lysis buffer via rotation at 4^{o}C for 4 hours. Antibody-Sepharose A coupled beads were washed 4 times in non-denaturing lysis buffer containing protease and phosphatase inhibitors with intermediate centrifugation steps as abovementioned. IP was performed via incubating 500 - 1000 µg of total cell protein extracts (into non-denaturing lysis buffer containing phosphatase and protease inhibitors) with 10 µl antibody-Sepharose A coupled beads in a total volume of 1000 µl with rotating for 3 hours at 4^{o} C. Then beads were washed 4 times with 1000 µl non-denaturing lysis buffer containing phosphatase and protease inhibitors followed by centrifugation for 20 sec at 13200 rpm. The pellet was resuspended in 50 µl of 1X protein loading buffer, incubated at 95^{o} C for 5 min and centrifuged at 13200 rpm for 1 min. The supernatant containing the immunoprecipitated proteins was then analysed using immunoblotting.

Phospho-RTK array

The human phospho-RTK array [#ARY001B (R&D Systems, Abingdon, UK)] was used for the determination of changes in phosphorylation of RTKs between autophagy-proficient and -compromised samples. The array was conducted with the specific reagents provided and based on the instructions of the manufacturer. Briefly, 1.5 - 2 x 10^{6} autophagy-proficient or -compromised cells (depending on the cell line used) were plated in 10 cm tissue culture dishes at day 3 of Dox treatment and let to adhere for another 48 hours at 37^{o}C in the presence of Dox. Then cells were lysed

using Lysis Buffer 17 supplemented with protease and phosphatase inhibitors and protein quantification of total cell extracts was conducted using Bradford assay. 1500 µg of total cell extracts was diluted into array buffer 1 to reach a volume of 1.5 ml and samples of each autophagy-proficient or -compromised condition were applied onto the nitrocellulose membrane with the RTK-captured antibodies. Followed overnight incubation at 4^{o}C on a rocking platform shaker and the next day nitrocellulose membranes were washed and incubated with a pan anti-phospho-tyrosine antibody conjugated to HRP in a dilution 1:5000 for 2 hours at room temperature. The phosphorylated tyrosines on RTKs were detected by chemilluminescence using X-ray Films and multiple exposure times (20 sec - 10 min) were used to detect the majority of RTKs. Nitrocellulose membranes incubated with autophagy-proficient or -compromised lysates were placed into the same autoradiography cassette and developed concomitantly to allow comparison between conditions. For densitometric analysis of phospho-RTK array results, X-ray films were scanned in high resolution (1200 dpi) and the GS-800 Calibrated Densitometer (BioRad) was used to quantify the intensity of each independent RTK spot. Numerical results were analysed by determining the average signal (pixel intensity) of the pair of duplicate spots presenting each RTK and followed by subtraction of an averaged background signal for each RTK independently. Differences in RTK phosphorylation were determined by comparing phosphorylation of RTKs between autophagy-proficient and -compromised cells.

Sulforhodamine B (SRB) Cell Proliferation / Survival assay

Using the Sulforhodamine B (SRB) colorimetric assay, cell proliferation/survival was assessed upon drug treatments. SRB assay is used for cell density determination by measuring cellular protein content.[83] 3000 cells / 200 µl of medium were seeded in each well of flat 96-well plates. 48 hours post-seeding cells were treated with the indicated concentration of Cetuximab -/+ 10 µM CQ for 87 hours at 37^{o} C. A separate

control plate that has been seeded with the same number of cells was fixed before treatment and considered as the “day 0” control. The control plate was stored at room temperature and processed along with the experimental plates. Briefly, media was aspirated from the wells and cells fixed in 10% (w/v) of Trichloroacetic acid for 20 min at 4^{o} C. Cells stained in 0.4% (w/v) SRB solution for 20 min at room temperature. Traces of the unbound dye were removed by washing cells 5 times with 1% (w/v) Trichloroacetic acid and the plates air-dried overnight. The dye was solubilized with 10 mM Tris base (pH 10.5) for 30 min at room temperature and absorbance was measured at 540 nm. Numerical results were analysed and expressed as % of control cell growth as previously described.[83]

Immunofluorescence (IF)

6 x 10^4 HCT-116 cells were plated on sterile glass coverslips in 24-well plates and let to adhere for 48 hours at 37^{o}C. Cells were treated with 10 μM CQ for 6 hours. Cells were fixed with 4% PFA for 15 min, followed incubation in 100% methanol for 10 min in -20^{o}C and finally three washes in 1X PBS (5 min each). Fixed cells were blocked in blocking buffer (5% BSA in 1X PBS supplemented with 0.3% Triton-X100) for 1 hour at room temperature and were stained with the corresponding primary antibody overnight at 4^{o} C. After primary antibody incubation, cells were washed 3 times with 1X PBS – 0.1% Tween-20 to remove traces of unspecifically bound antibody and followed incubation in dark with secondary fluorescent-conjugated antibodies at room temperature for 1 hour. Traces of secondary antibody were removed by washing 3 times with 1X PBS – 0.1% Tween-20. Nuclear staining was performed via incubating cells with Hoechst dye in a dilution 1:5000 in PBS for 30 min. Coverslips were mounted on microscope slides, let to dry and stored at 4^{o} C. Images were acquired using a Zeiss LSM 700 (Carl Zeiss Microscopy Ltd, Cambridge, UK) confocal microscope using x63 objective/1.4 numerical aperture. Z-stack images thickness was set to 0.4 μm and images in each experiment were acquired at same settings

and exposure times. Post-acquisition brightness adjustments were identical between images of the same experiment and performed in Adobe Photoshop (Adobe Systems, San Jose, CA, USA). Quantification of intracellular c-MET was performed by manually specifying the intracellular region of interest (ROI) of every cell in a single z-stack image using Fiji software. Plasma membrane staining was excluded from quantification analysis.

Determination of *KRAS* and *PIK3CA* mutational status

2 x 10^6 CRC cells were harvested by trypsinisation, pelleted down and subjected to RNA extraction by using the RNeasy Plus Mini Kit [#74134, Qiagen Ltd, (Manchester, UK)]. The procedure conducted based on the instructions of the manufacturer. Total RNA was eluted in 30 µl RNase-free H_2O. The high capacity cDNA reverse transcription kit (#4368814, Thermo Fisher Scientific) was used to retrotranscribe 1 µg of RNA isolated from CRC cells based on the instructions of the manufacturer. Briefly, reverse-transcription PCR reaction was performed in a total volume of 20 µl containing RNA and 2X RT mastermix (10X RT buffer; 25X dNTP Mix; 10X RT random primers; multiscribe reverse transcriptase; RNA inhibitors; nuclease-free H_2O) in a 1:1 ratio. The conditions of reverse-transcription PCR were 25^o C for 10 min, 37^o C for 120 min and 85^o C for 5 min.

The newly synthesized cDNA was used with each of the following primer pairs for *KRAS* and *PIK3CA* mutational status determination using PCR.

*KRAS*_Exon1-2 forward primer: AGGCCTGCTGAAAATGACTGAA

*KRAS*_Exon3 reverse primer: GGTCCCTCATTGCACTGTACTCC

*PIK3CA*_Exon15-16 forward primer: ATGATTTACGGCAAGATATGC

*PIK3CA*_Exon20 reverse primer: TCAGTTCAATGCATGCTGTTT

*PIK3CA*_Exon4-5 forward primer: AAGATCTATGTTCGAACAGGT

*PIK3CA*_Exon11-10 reverse primer: ACATCTGGGCTACTTCATCTC

PCR reactions were performed in a total volume of 50 µl, containing 5 µM of each forward and reverse primers, 46 µl PCR Master Mix ($MgCl_2$ buffer; dNTPs; nuclease-free H_2O) with 1 Unit of FastStart Taq DNA Polymerase (Roche). The conditions of PCR reactions were for *KRAS* fragments: 35 cycles of 95° C for 1 min, 62.1° C for 45 sec and 72° C for 45 sec with an initial denaturation cycle of 95° C for 5 min and a final extension cycle of 70° C for 7 min; and *PIK3CA* fragments: 35 cycles of 95° C for 1 min, 60° C for 45 sec and 72° C for 1 min with an initial denaturation cycle of 95° C for 5 min and a final extension cycle of 72° C for 10 min. Fractionation of PCR products was performed by electrophoresis in 1 - 1.5% Agarose (#A9539, Sigma) / TAE gel containing ethidium bromide. DNA was mixed with 5X DNA Loading Buffer [100 mM Tris pH 8; 10 mM EDTA pH 8; 50% Glycerol; 0.5% (w/v) bromophenol blue] and electrophoresed at 100 V for approximately 30 min. DNA bands were visualised under ultraviolet light. Purification of DNA fragments from Agarose / TAE gel was performed by GeneJet Gel Extraction kit (#K0691, Thermo Fisher Scientific) following the instructions of the manufacturer. Sequencing of PCR amplified fragments was performed in the UCL CI sequencing facility by using the appropriate primers. Sequencing results were visualised using Finch TV software and were further analysed by using the EMBOSS Pairwise Alignment Algorithm from the EMBL-EBI Database (http://www.ebi.ac.uk/Tools/emboss/align/).

Cloning of shRNA oligos to pLKO-Tet-On vector

To generate shRNA pLKO-Tet-On expressing plasmids against ATG7 protein, single-stranded oligos encoding the desired shRNA sequence were designed based on previously published shATG7 sequences.[29] ATG7 single-stranded oligo sequences were incorporated with cloning overhangs and loop sequence. ATG7 single-stranded oligos firstly annealed and then cloned into the inducible lentiviral pLKO-Tet-On vector by following the previously described protocols.[80, 82] For the annealing of

single-stranded oligos, 11.25 µl of each forward and reverse oligo (100 µM) were mixed with 2.5 µl of 10X annealing buffer (1 M NaCl; 100 mM Tris-HCl, pH 7.4) and a PCR program was used to perform the reaction. The conditions of the PCR program used are: 10 min at 98° C, 5 min at 95° C, 5 min at 90° C, 5 min at 88° C, 5 min at 85° C, 5 min at 80° C, 5 min at 78° C, 5 min at 75° C, 5 min at 70° C, 5 min at 68° C, 5 min at 65° C, 5 min at 60° C, 5 min at 58° C, 5 min at 55° C, 5 min at 50° C, 5 min at 45° C, 5 min at 40° C, 10 min at 37° C and cooling down to 4° C. The annealed oligo mixture was diluted in 0.5X of annealing buffer in a ratio 1:400 and ligated to the cloning sites of pLKO-Tet-On vector created by *AgeI* (Promega Corp., Madison, WI, USA) /*EcoRI* (Roche) digestion in Multicore buffer (Promega). The reaction was incubated at 37° C for $1^{1/2}$ hours and the restriction digestion products were visualised on 1% Agarose / TAE gel. Followed purification of the digested pLKO-Tet-On vector from Agarose / TAE gel by following the instructions of the manufacturer (GeneJet Gel Extraction kit; #K0691; Thermo Fisher Scientific). Ligation reaction was performed in a total volume of 10 µl, containing double-stranded oligos, the digested pLKO-Tet-On vector, 2X Rapid Ligase buffer (#C671B, Promega) and T4 DNA ligase (#M180B, Promega). Ligation mixture was incubated at room temperature for 15 min and transformation of ligated products in Stbl3 cells followed. Bacteria colonies were grown to enable purification of plasmid DNA using the JetStar 2.0 Plasmid Purification Kit (Genomed, Löhne, Germany) according to the instructions of the manufacturer. Verification of the inserted oligos was conducted by sequencing.

Cloning of guide RNA sequences to lentiCRISPR vector

The target guide RNA sequence against human *ATG7* was designed based on the Zhang Lab GeCKO website http://www.genome-engineering.org/gecko/. Additionally, the CRISPR design tool software http://crispr.mit.edu/ was used for the identification of suitable target sites for guide RNA sequence design against *ATG7*. For targeting ATG7, the exon 2 coding sequence: GAAGCTGAACGAGTATCGGC was used. For

control (Ctrl), the gRNA sequence GTAGCGAACGTGTCCGGCGT was used, generated by Wang *et al.*[84] The abovementioned oligo-sequences integrated with specific overhangs for cloning were ordered.

To clone the Ctrl and ATG7 gRNA sequences, 5 µg of the lentiCRISPR vector was enzymatically digested with *BsmBI* (NEB) using Buffer 3.1 (NEB) for 2 hours at 37° C. 10 µM of each single-stranded forward and reverse -gRNA oligo was phosphorylated using T4 Polynucleotide Kinase (Cambio) at 37° C for 30 min (based on the instructions of the manufacturer) and then annealed by heating at 95° C for 5 min and cooling down to 25° C at 5° C/min. The annealed gRNA oligos were diluted in a 1/200 concentration using ddH_2O and ligated into 50 ng gel purified vector (QIAquick Gel Extraction Kit; #28704, Qiagen). For ligation reaction, the Rapid DNA Ligation kit (#11 635 379 001, Roche) was used at room temperature for 15min according to the instructions of the manufacturer. Followed transformation of ligated products in Stbl3 cells. Bacteria colonies were grown and purification of plasmid DNA from mini-cultures was performed. Verification of gRNA cloning was conducted by sequencing using .the LKO.1 forward primer: 5'- GACTATCATATGCTTACCGT-3'. Positive clones were amplified in large-volume bacteria cultures and plasmid DNA was isolated for long-term storage and use.

Statistical analysis

Means of at least three independent experiments unless otherwise stated were statistically analysed using GraphPad Prism v5 (GraphPad Software, Inc, La Jolla, CA, USA). Determination of statistical significance in single-comparisons was performed using two-tailed unpaired Student's t-test with Welch's correction and in multiple means comparisons using one-way or two-way ANOVA followed by the Bonferroni post-test.

Acknowledgements

We thank Dr Pablo Rodriguez-Viciana (University College London, UK), Dr Ivana Bjedov (University College London, UK), Prof. Bart Vanhaesebroeck (University College London, UK), Dr Benoit Bilanges (University College London, UK), Prof Clare Futter (University College London, UK), Prof. Bert Vogelstein (Johns Hopkins University, USA), Prof. Alberto Bardelli (University of Torino, Italy) for reagents. A special thanks also to all members of PS and DH labs and the CRUK UCL Centre Core Services and the UCL Scientific Services. AL was recipient of a PhD studentship award from the UCL Grand Challenges. DH was supported by Cancer Research UK Programme Grant (C2259/A16569). PS is head of the Brain Tumour Charity-funded Samantha Dickson Brain Cancer Unit.

Conflict of Interest

The authors declare no conflict of interest.

Supplementary Information accompanies this paper on Cell Death and Differentiation website (http://www.nature.com/cdd).

References

1. Mizushima N, Levine B, Cuervo AM, Klionsky DJ. Autophagy fights disease through cellular self-digestion. Nature. 2008 Feb 28;451(7182):1069-75. PubMed PMID: 18305538. Pubmed Central PMCID: 2670399.

2. Ravikumar B, Sarkar S, Davies JE, Futter M, Garcia-Arencibia M, Green-Thompson ZW, *et al.* Regulation of mammalian autophagy in physiology and pathophysiology. Physiological reviews. 2010 Oct;90(4):1383-435. PubMed PMID: 20959619.

3. Mizushima N, Komatsu M. Autophagy: renovation of cells and tissues. Cell. 2011 Nov 11;147(4):728-41. PubMed PMID: 22078875.

4. Feng Y, He D, Yao Z, Klionsky DJ. The machinery of macroautophagy. Cell research. 2014 Jan;24(1):24-41. PubMed PMID: 24366339. Pubmed Central PMCID: 3879710.

5. He C, Klionsky DJ. Regulation mechanisms and signaling pathways of autophagy. Annual review of genetics. 2009;43:67-93. PubMed PMID: 19653858. Pubmed Central PMCID: 2831538.

6. Kroemer G, Marino G, Levine B. Autophagy and the integrated stress response. Molecular cell. 2010 Oct 22;40(2):280-93. PubMed PMID: 20965422. Pubmed Central PMCID: 3127250.

7. Efeyan A, Comb WC, Sabatini DM. Nutrient-sensing mechanisms and pathways. Nature. 2015 01/15/print;517(7534):302-10.

8. Heras-Sandoval D, Perez-Rojas JM, Hernandez-Damian J, Pedraza-Chaverri J. The role of PI3K/AKT/mTOR pathway in the modulation of autophagy and the clearance of protein aggregates in neurodegeneration. Cellular signalling. 2014 Dec;26(12):2694-701. PubMed PMID: 25173700.

9. Laplante M, Sabatini David M. mTOR Signaling in Growth Control and Disease. Cell. 2012 4/13/;149(2):274-93.

10. Russell RC, Yuan HX, Guan KL. Autophagy regulation by nutrient signaling. Cell research. 2014 Jan;24(1):42-57. PubMed PMID: 24343578. Pubmed Central PMCID: 3879708.

11. Yang Z, Klionsky DJ. Mammalian autophagy: core molecular machinery and signaling regulation. Current Opinion in Cell Biology. 2010 4//;22(2):124-31.

12. Kim Y-M, Jung Chang H, Seo M, Kim Eun K, Park J-M, Bae Sun S*, et al.* mTORC1 Phosphorylates UVRAG to Negatively Regulate Autophagosome and Endosome Maturation. Molecular cell. 2015 1/22/;57(2):207-18.

13. Dou Z, Pan JA, Dbouk HA, Ballou LM, DeLeon JL, Fan Y*, et al.* Class IA PI3K p110beta subunit promotes autophagy through Rab5 small GTPase in response to growth factor limitation. Molecular cell. 2013 Apr 11;50(1):29-42. PubMed PMID: 23434372. Pubmed Central PMCID: 3628298.

14. Guo JY, Chen HY, Mathew R, Fan J, Strohecker AM, Karsli-Uzunbas G*, et al.* Activated Ras requires autophagy to maintain oxidative metabolism and tumorigenesis. Genes & development. 2011 Mar 1;25(5):460-70. PubMed PMID: 21317241. Pubmed Central PMCID: 3049287.

15. Perera RM, Stoykova S, Nicolay BN, Ross KN, Fitamant J, Boukhali M*, et al.* Transcriptional control of autophagy-lysosome function drives pancreatic cancer metabolism. Nature. 2015 08/20/print;524(7565):361-5.

16. Sarkar S. Regulation of autophagy by mTOR-dependent and mTOR-independent pathways: autophagy dysfunction in neurodegenerative diseases and therapeutic application of autophagy enhancers. Biochemical Society transactions. 2013 Oct;41(5):1103-30. PubMed PMID: 24059496.

17. Tan X, Thapa N, Sun Y, Anderson Richard A. A Kinase-Independent Role for EGF Receptor in Autophagy Initiation. Cell. 2015 1/15/;160(1–2):145-60.

18. Wang RC, Wei Y, An Z, Zou Z, Xiao G, Bhagat G*, et al.* Akt-Mediated Regulation of Autophagy and Tumorigenesis Through Beclin 1 Phosphorylation. Science. 2012 November 16, 2012;338(6109):956-9.

19. Wei Y, Zou Z, Becker N, Anderson M, Sumpter R, Xiao G*, et al.* EGFR-Mediated Beclin 1 Phosphorylation in Autophagy Suppression, Tumor Progression, and Tumor Chemoresistance. Cell. 2013 9/12/;154(6):1269-84.

20. Karantza-Wadsworth V, Patel S, Kravchuk O, Chen G, Mathew R, Jin S*, et al.* Autophagy mitigates metabolic stress and genome damage in mammary tumorigenesis. Genes & development. 2007 Jul 1;21(13):1621-35. PubMed PMID: 17606641. Pubmed Central PMCID: 1899472.

21. Liang XH, Jackson S, Seaman M, Brown K, Kempkes B, Hibshoosh H*, et al.* Induction of autophagy and inhibition of tumorigenesis by beclin 1. Nature. 1999 Dec 9;402(6762):672-6. PubMed PMID: 10604474.

22. Mathew R, Karp CM, Beaudoin B, Vuong N, Chen G, Chen HY*, et al.* Autophagy suppresses tumorigenesis through elimination of p62. Cell. 2009 Jun 12;137(6):1062-75. PubMed PMID: 19524509. Pubmed Central PMCID: 2802318.

23. Mathew R, Kongara S, Beaudoin B, Karp CM, Bray K, Degenhardt K*, et al.* Autophagy suppresses tumor progression by limiting chromosomal instability. Genes & development. 2007 Jun 1;21(11):1367-81. PubMed PMID: 17510285. Pubmed Central PMCID: 1877749.

24. Qu X, Yu J, Bhagat G, Furuya N, Hibshoosh H, Troxel A*, et al.* Promotion of tumorigenesis by heterozygous disruption of the beclin 1 autophagy gene. The Journal of clinical investigation. 2003 Dec;112(12):1809-20. PubMed PMID: 14638851. Pubmed Central PMCID: 297002.

25. Rosenfeldt MT, Ryan KM. The multiple roles of autophagy in cancer. Carcinogenesis. 2011 Jul;32(7):955-63. PubMed PMID: 21317301. Pubmed Central PMCID: 3128556.

26. Takamura A, Komatsu M, Hara T, Sakamoto A, Kishi C, Waguri S*, et al.* Autophagy-deficient mice develop multiple liver tumors. Genes & development. 2011 Apr 15;25(8):795-800. PubMed PMID: 21498569. Pubmed Central PMCID: 3078705.

27. White E. Deconvoluting the context-dependent role for autophagy in cancer. Nature reviews Cancer. 2012 Jun;12(6):401-10. PubMed PMID: 22534666. Pubmed Central PMCID: 3664381.

28. Bellodi C, Lidonnici MR, Hamilton A, Helgason GV, Soliera AR, Ronchetti M*, et al.* Targeting autophagy potentiates tyrosine kinase inhibitor-induced cell death in Philadelphia chromosome-positive cells, including primary CML stem cells. The Journal of clinical investigation. 2009 May;119(5):1109-23. PubMed PMID: 19363292. Pubmed Central PMCID: 2673867.

29. Galavotti S, Bartesaghi S, Faccenda D, Shaked-Rabi M, Sanzone S, McEvoy A*, et al.* The autophagy-associated factors DRAM1 and p62 regulate cell migration and invasion in glioblastoma stem cells. Oncogene. 2013 Feb 7;32(6):699-712. PubMed PMID: 22525272.

30. Guo JY, Karsli-Uzunbas G, Mathew R, Aisner SC, Kamphorst JJ, Strohecker AM*, et al.* Autophagy suppresses progression of K-ras-induced lung tumors to oncocytomas and maintains lipid homeostasis. Genes & development. 2013 July 1, 2013;27(13):1447-61.

31. Levy J, Cacheux W, Bara MA, L'Hermitte A, Lepage P, Fraudeau M*, et al.* Intestinal inhibition of Atg7 prevents tumour initiation through a microbiome-influenced immune response and suppresses tumour growth. Nature cell biology. 2015 Aug;17(8):1062-73. PubMed PMID: 26214133.

32. Rao S, Tortola L, Perlot T, Wirnsberger G, Novatchkova M, Nitsch R*, et al.* A dual role for autophagy in a murine model of lung cancer. Nat Commun. 2014 01/20/online;5.

33. Rosenfeldt MT, O'Prey J, Morton JP, Nixon C, MacKay G, Mrowinska A*, et al.* p53 status determines the role of autophagy in pancreatic tumour development. Nature. 2013 Dec 12;504(7479):296-300. PubMed PMID: 24305049.

34. Strohecker AM, Guo JY, Karsli-Uzunbas G, Price SM, Chen GJ, Mathew R*, et al.* Autophagy Sustains Mitochondrial Glutamine Metabolism and Growth of BrafV600E–Driven Lung Tumors. Cancer Discovery. 2013 November 1, 2013;3(11):1272-85.

35. Strohecker AM, White E. Autophagy promotes BrafV600E-driven lung tumorigenesis by preserving mitochondrial metabolism. Autophagy. 2014 Feb;10(2):384-5. PubMed PMID: 24362353.

36. Yang A, Rajeshkumar NV, Wang X, Yabuuchi S, Alexander BM, Chu GC*, et al.* Autophagy is critical for pancreatic tumor growth and progression in tumors with

p53 alterations. Cancer Discov. 2014 Aug;4(8):905-13. PubMed PMID: 24875860. Pubmed Central PMCID: 4125497.

37. Galluzzi L, Pietrocola F, Bravo-San Pedro JM, Amaravadi RK, Baehrecke EH, Cecconi F*, et al.* Autophagy in malignant transformation and cancer progression. The EMBO journal. 2015 Apr 1;34(7):856-80. PubMed PMID: 25712477. Pubmed Central PMCID: 4388596.

38. Amaravadi RK, Lippincott-Schwartz J, Yin XM, Weiss WA, Takebe N, Timmer W*, et al.* Principles and current strategies for targeting autophagy for cancer treatment. Clinical cancer research : an official journal of the American Association for Cancer Research. 2011 Feb 15;17(4):654-66. PubMed PMID: 21325294. Pubmed Central PMCID: 3075808.

39. Calabretta B, Salomoni P. Inhibition of autophagy: a new strategy to enhance sensitivity of chronic myeloid leukemia stem cells to tyrosine kinase inhibitors. Leukemia & lymphoma. 2011 Feb;52 Suppl 1:54-9. PubMed PMID: 21250825.

40. Ma X-H, Piao S-F, Dey S, McAfee Q, Karakousis G, Villanueva J*, et al.* Targeting ER stress–induced autophagy overcomes BRAF inhibitor resistance in melanoma. The Journal of clinical investigation. 2014;124(3):1406-17.

41. Wu Z, Chang PC, Yang JC, Chu CY, Wang LY, Chen NT*, et al.* Autophagy Blockade Sensitizes Prostate Cancer Cells towards Src Family Kinase Inhibitors. Genes & cancer. 2010 Jan;1(1):40-9. PubMed PMID: 20811583. Pubmed Central PMCID: 2930266.

42. Dragowska WH, Weppler SA, Wang JC, Wong LY, Kapanen AI, Rawji JS*, et al.* Induction of autophagy is an early response to gefitinib and a potential therapeutic target in breast cancer. PloS one. 2013;8(10):e76503. PubMed PMID: 24146879. Pubmed Central PMCID: 3795739.

43. Eimer S, Belaud-Rotureau MA, Airiau K, Jeanneteau M, Laharanne E, Veron N*, et al.* Autophagy inhibition cooperates with erlotinib to induce glioblastoma cell

death. Cancer biology & therapy. 2011 Jun 15;11(12):1017-27. PubMed PMID: 21508666.

44. Gorzalczany Y, Gilad Y, Amihai D, Hammel I, Sagi-Eisenberg R, Merimsky O. Combining an EGFR directed tyrosine kinase inhibitor with autophagy-inducing drugs: a beneficial strategy to combat non-small cell lung cancer. Cancer letters. 2011 Nov 28;310(2):207-15. PubMed PMID: 21807458.

45. Han W, Pan H, Chen Y, Sun J, Wang Y, Li J*, et al.* EGFR tyrosine kinase inhibitors activate autophagy as a cytoprotective response in human lung cancer cells. PloS one. 2011;6(6):e18691. PubMed PMID: 21655094. Pubmed Central PMCID: 3107207.

46. Li X, Fan Z. The epidermal growth factor receptor antibody cetuximab induces autophagy in cancer cells by downregulating HIF-1alpha and Bcl-2 and activating the beclin 1/hVps34 complex. Cancer research. 2010 Jul 15;70(14):5942-52. PubMed PMID: 20634405. Pubmed Central PMCID: 2933174.

47. Li X, Lu Y, Pan T, Fan Z. Roles of autophagy in cetuximab-mediated cancer therapy against EGFR. Autophagy. 2010 Nov;6(8):1066-77. PubMed PMID: 20864811. Pubmed Central PMCID: 3039478.

48. Li Y-y, Lam S-k, Mak JC-w, Zheng C-y, Ho JC-m. Erlotinib-induced autophagy in epidermal growth factor receptor mutated non-small cell lung cancer. Lung Cancer.81(3):354-61.

49. Tang MC, Wu MY, Hwang MH, Chang YT, Huang HJ, Lin AM*, et al.* Chloroquine enhances gefitinib cytotoxicity in gefitinib-resistant nonsmall cell lung cancer cells. PloS one. 2015;10(3):e0119135. PubMed PMID: 25807554. Pubmed Central PMCID: 4373825.

50. Zou Y, Ling Y-H, Sironi J, Schwartz EL, Perez-Soler R, Piperdi B. The autophagy inhibitor chloroquine overcomes the innate resistance to erlotinib of non-small cell lung cancer cells with wild-type EGFR. Journal of thoracic oncology :

official publication of the International Association for the Study of Lung Cancer. 2013;8(6):10.1097/JTO.0b013e31828c7210. PubMed PMID: PMC3855301.

51. Humbert M, Medová M, Aebersold DM, Blaukat A, Bladt F, Fey MF*, et al.* Protective autophagy is involved in resistance towards MET inhibitors in human gastric adenocarcinoma cells. Biochemical and Biophysical Research Communications. 2013 2/8/;431(2):264-9.

52. Samame Perez-Vargas JC, Biondani P, Maggi C, Gariboldi M, Gloghini A, Inno A*, et al.* Role of cMET in the development and progression of colorectal cancer. International journal of molecular sciences. 2013;14(9):18056-77. PubMed PMID: 24005867. Pubmed Central PMCID: 3794769.

53. Bardelli A, Corso S, Bertotti A, Hobor S, Valtorta E, Siravegna G*, et al.* Amplification of the MET receptor drives resistance to anti-EGFR therapies in colorectal cancer. Cancer Discov. 2013 Jun;3(6):658-73. PubMed PMID: 23729478.

54. Misale S, Di Nicolantonio F, Sartore-Bianchi A, Siena S, Bardelli A. Resistance to Anti-EGFR Therapy in Colorectal Cancer: From Heterogeneity to Convergent Evolution. Cancer Discovery. 2014 November 1, 2014;4(11):1269-80.

55. Radinsky R, Risin S, Fan D, Dong Z, Bielenberg D, Bucana CD*, et al.* Level and function of epidermal growth factor receptor predict the metastatic potential of human colon carcinoma cells. Clinical cancer research : an official journal of the American Association for Cancer Research. 1995 Jan;1(1):19-31. PubMed PMID: 9815883.

56. Spano JP, Fagard R, Soria JC, Rixe O, Khayat D, Milano G. Epidermal growth factor receptor signaling in colorectal cancer: preclinical data and therapeutic perspectives. Annals of oncology : official journal of the European Society for Medical Oncology / ESMO. 2005 Feb;16(2):189-94. PubMed PMID: 15668269.

57. Sato K, Tsuchihara K, Fujii S, Sugiyama M, Goya T, Atomi Y*, et al.* Autophagy is activated in colorectal cancer cells and contributes to the tolerance to

nutrient deprivation. Cancer research. 2007 Oct 15;67(20):9677-84. PubMed PMID: 17942897.

58. Heinemann V, Douillard JY, Ducreux M, Peeters M. Targeted therapy in metastatic colorectal cancer -- an example of personalised medicine in action. Cancer treatment reviews. 2013 Oct;39(6):592-601. PubMed PMID: 23375249.

59. Santoro V, Jia R, Thompson H, Nijhuis A, Jeffery R, Kiakos K*, et al.* Role of Reactive Oxygen Species in the Abrogation of Oxaliplatin Activity by Cetuximab in Colorectal Cancer. Journal of the National Cancer Institute. 2016 Jun;108(6):djv394. PubMed PMID: 26719345. Pubmed Central PMCID: 4864961.

60. Gschwind A, Fischer OM, Ullrich A. The discovery of receptor tyrosine kinases: targets for cancer therapy. Nature reviews Cancer. 2004 05//print;4(5):361-70.

61. Lemmon MA, Schlessinger J. Cell signaling by receptor tyrosine kinases. Cell. 2010 Jun 25;141(7):1117-34. PubMed PMID: 20602996. Pubmed Central PMCID: 2914105.

62. De Roock W, De Vriendt V, Normanno N, Ciardiello F, Tejpar S. KRAS, BRAF, PIK3CA, and PTEN mutations: implications for targeted therapies in metastatic colorectal cancer. The lancet oncology. 2011 Jun;12(6):594-603. PubMed PMID: 21163703.

63. Klionsky DJ, Abdelmohsen K, Abe A, Abedin MJ, Abeliovich H, Acevedo Arozena A*, et al.* Guidelines for the use and interpretation of assays for monitoring autophagy (3rd edition). Autophagy. 2016;12(1):1-222. PubMed PMID: 26799652. Pubmed Central PMCID: 4835977.

64. Vanhaesebroeck B, Guillermet-Guibert J, Graupera M, Bilanges B. The emerging mechanisms of isoform-specific PI3K signalling. Nat Rev Mol Cell Biol. 2010 05//print;11(5):329-41.

65. Roberts PJ, Der CJ. Targeting the Raf-MEK-ERK mitogen-activated protein kinase cascade for the treatment of cancer. Oncogene. 2007 May 14;26(22):3291-310. PubMed PMID: 17496923.

66. Klippel A, Reinhard C, Kavanaugh WM, Apell G, Escobedo MA, Williams LT. Membrane localization of phosphatidylinositol 3-kinase is sufficient to activate multiple signal-transducing kinase pathways. Molecular and Cellular Biology. 1996;16(8):4117-27. PubMed PMID: PMC231408.

67. Komatsu M, Kageyama S, Ichimura Y. p62/SQSTM1/A170: physiology and pathology. Pharmacological research. 2012 Dec;66(6):457-62. PubMed PMID: 22841931.

68. Martinez-Lopez N, Athonvarangkul D, Mishall P, Sahu S, Singh R. Autophagy proteins regulate ERK phosphorylation. Nat Commun. 2013 11/18/online;4.

69. Bernard M, Dieudé M, Yang B, Hamelin K, Underwood K, Hébert M-J. Autophagy fosters myofibroblast differentiation through MTORC2 activation and downstream upregulation of CTGF. Autophagy. 2014 2014/12/02;10(12):2193-207.

70. Peruzzi B, Bottaro DP. Targeting the c-Met Signaling Pathway in Cancer. Clinical Cancer Research. 2006 June 15, 2006;12(12):3657-60.

71. Sandilands E, Serrels B, Wilkinson S, Frame MC. Src-dependent autophagic degradation of Ret in FAK-signalling-defective cancer cells. EMBO reports. 2012 Aug;13(8):733-40. PubMed PMID: 22732841. Pubmed Central PMCID: 3410392.

72. Jones S, Cunningham DL, Rappoport JZ, Heath JK. The non-receptor tyrosine kinase Ack1 regulates the fate of activated EGFR by inducing trafficking to the p62/NBR1 pre-autophagosome. Journal of Cell Science. 2014 March 1, 2014;127(5):994-1006.

73. Humphrey SJ, Yang G, Yang P, Fazakerley DJ, Stockli J, Yang JY*, et al.* Dynamic adipocyte phosphoproteome reveals that Akt directly regulates mTORC2. Cell metabolism. 2013 Jun 4;17(6):1009-20. PubMed PMID: 23684622. Pubmed Central PMCID: 3690479.

74. Yin Y, Hua H, Li M, Liu S, Kong Q, Shao T*, et al.* mTORC2 promotes type I insulin-like growth factor receptor and insulin receptor activation through the tyrosine kinase activity of mTOR. Cell research. 2016 Jan;26(1):46-65. PubMed PMID: 26584640. Pubmed Central PMCID: 4816127.

75. Dibble CC, Asara JM, Manning BD. Characterization of Rictor phosphorylation sites reveals direct regulation of mTOR complex 2 by S6K1. Mol Cell Biol. 2009 Nov;29(21):5657-70. PubMed PMID: 19720745. Pubmed Central PMCID: 2772744.

76. Julien LA, Carriere A, Moreau J, Roux PP. mTORC1-activated S6K1 phosphorylates Rictor on threonine 1135 and regulates mTORC2 signaling. Mol Cell Biol. 2010 Feb;30(4):908-21. PubMed PMID: 19995915. Pubmed Central PMCID: 2815569.

77. Liu P, Gan W, Inuzuka H, Lazorchak AS, Gao D, Arojo O*, et al.* Sin1 phosphorylation impairs mTORC2 complex integrity and inhibits downstream Akt signalling to suppress tumorigenesis. Nature cell biology. 2013 Nov;15(11):1340-50. PubMed PMID: 24161930. Pubmed Central PMCID: 3827117.

78. Xie J, Proud CG. Signaling crosstalk between the mTOR complexes. Translation. 2014;2(1):e28174. PubMed PMID: 26779402. Pubmed Central PMCID: 4705829.

79. Arias E, Koga H, Diaz A, Mocholi E, Patel B, Cuervo Ana M. Lysosomal mTORC2/PHLPP1/Akt Regulate Chaperone-Mediated Autophagy. Molecular cell.59(2):270-84.

80. Wiederschain D, Wee S, Chen L, Loo A, Yang G, Huang A*, et al.* Single-vector inducible lentiviral RNAi system for oncology target validation. Cell cycle. 2009 Feb 1;8(3):498-504. PubMed PMID: 19177017.

81. Sanjana NE, Shalem O, Zhang F. Improved vectors and genome-wide libraries for CRISPR screening. Nature methods. 2014 Aug;11(8):783-4. PubMed PMID: 25075903. Pubmed Central PMCID: 4486245.

82. Wee S, Wiederschain D, Maira SM, Loo A, Miller C, deBeaumont R*, et al.* PTEN-deficient cancers depend on PIK3CB. Proceedings of the National Academy of Sciences of the United States of America. 2008 Sep 2;105(35):13057-62. PubMed PMID: 18755892. Pubmed Central PMCID: 2529105.

83. Vichai V, Kirtikara K. Sulforhodamine B colorimetric assay for cytotoxicity screening. Nature protocols. 2006;1(3):1112-6. PubMed PMID: 17406391.

84. Wang T, Wei JJ, Sabatini DM, Lander ES. Genetic screens in human cells using the CRISPR-Cas9 system. Science. 2014 Jan 3;343(6166):80-4. PubMed PMID: 24336569. Pubmed Central PMCID: 3972032.

Figure legends

Figure 1 The majority of CRC cells are incompetent for autophagy induction following EGFR targeted therapy but they have basal levels of autophagy. (**a-e**) Autophagy induction following EGFR targeted therapy in CRC cells. CRC cells [(**a**) DiFi; (**b**) HCT-116; (**c**) CaCo2; (**d**) DLD-1 and (**e**) SW48] were treated with 50 or 100 μg/ml Cetuximab +/- 10 μM CQ for 24 hours and total cell lysates were analysed using immunoblot for LC3B protein. Autophagy induction in untreated and Cetuximab-treated CRC cells in the presence and/or absence of CQ was assessed by accumulation of LC3-II levels over LC3-I levels. Bar plots represent densitometric analysis of LC3-II/LC3-I levels normalised to β-actin or calnexin (n=1). (**f-i**) Monitoring of basal autophagic flux in CRC cell lines. CRC cells [(**f**) HCT-116; (**g**) DLD-1; (**h**) CaCo2 and (**i**) DiFi] were treated +/- 10μM CQ for 6 hours and total cell lysates were analysed using immunoblot for LC3B protein. Accumulation of LC3-II over LC3-I band following CQ treatment depicts basal autophagic flux of CRC cells (n=1). Levels of β-actin or calnexin were used as immunoblot loading controls.

Figure 2 Genetic modulation of autophagy reduces phosphorylation of RTKs in HCT-116 *KRAS* WT and G13D isogenic cells. Autophagy-proficient (shEGFP) and autophagy-compromised (shATG7 E8) cells were treated with 10 ng/ml Dox for 5 days to efficiently downregulate ATG7 protein and total cell lysates were subjected to phospho-RTK array analysis. (**a**) Immunoblots presented are from one complete experiment, processed simultaneously for all conditions examined and are representative of two independent experiments for *KRAS* WT and one experiment for *KRAS* G13D cells. Arrow indicates increased exposure time used to develop immunoblots. (**b-c**) Bar plots depict densitometric quantification of phospho-RTK array spots. Bars represent mean ± standard deviation. Black boxes indicate RTKs found to be deregulated upon autophagy suppression in both HCT-116 *KRAS* WT (**b**) and G13D (**c**) cells.

Figure 3 Autophagy inhibition downregulates c-MET RTK activation in CRC cells. (**a**) Total c-MET immunoprecipitation showing reduced c-MET phosphorylation in autophagy-compromised HCT-116 *KRAS* WT cells. Autophagy-proficient (shEGFP) and -compromised (shATG7 E8) cells 5 days after 10 ng/ml Dox treatment were lysed and total c-MET protein subjected to immunoprecipitation. Immunoprecipitated c-MET phosphorylation was assessed using immunoblotting for p-Tyrosine 4G10 antibody. Total c-MET was used to examine immunoprecipitation efficiency and loading. β-actin was used as loading control of total cell lysates (n=1). (**b**) Immunoblot showing reduced phosphorylation of c-MET Y1234/1235 catalytic subunit residues in autophagy-compromised HCT-116 *KRAS* WT and G13D cells. Autophagy-proficient (shEGFP) and -compromised (shATG7 E8) cells were treated with 10 ng/ml Dox for 5 days and total cell lysates were subjected to immunoblotting for ATG7, p-c-MET Y1234/1235 and total c-MET protein levels. β-actin was used as loading control. Bar plots represent densitometric quantification of p-c-MET Y1234/1235 relative to total c-MET protein. The bars represent mean ± standard deviation of n=3 (HCT-116 *KRAS* WT) and n=2 (HCT-116 *KRAS* G13D); * $p<0.05$. Unpaired Student's t-test statistical analysis was used for HCT-116 *KRAS* WT cells (n=3). (**c**) Immunoblot showing reduced phosphorylation of c-MET Y1234/1235 catalytic subunit residues in autophagy-deficient HCT-116 cells. Total cell lysates of autophagy-proficient (CRISPR Ctrl) and -deficient (CRISPR ATG7) cells were subjected to immunoblotting for ATG7, p-c-MET Y1234/1235 and total c-MET protein levels. Bar plot represents densitometric quantification of p-c-MET Y1234/1235 relative to total c-MET protein. The bars represent mean ± standard deviation of n=4; *** $p<0.001$. Unpaired Student's t-test statistical analysis was used. (**d**) Immunoblot

showing reduced phosphorylation of c-MET Y1234/1235 catalytic subunit residues in autophagy-compromised CaCo2 cells. Autophagy-proficient (shEGFP) and -compromised (shATG7 E8 and G7) cells were treated with 100 ng/ml Dox for 5 days and total cell lysates were subjected to immunoblotting for ATG7, p-c-MET Y1234/1235 and total c-MET protein levels. Bar plots represent densitometric quantification of p-c-MET Y1234/1235 relative to total c-MET protein. The bars represent mean ± standard deviation of n=2.

Figure 4 c-MET colocalises with LC3B positive intracellular structures but basal autophagy suppression does not alter c-MET intracellular accumulation. (**a**) Representative immunofluorescence images showing total c-MET colocalising with LC3B positive intracellular structures only in autophagy-proficient conditions. Autophagy-proficient (shEGFP) HCT-116 *KRAS* WT cells were treated with 10 ng/ml Dox for 5 days. At day 5 of Dox treatment, cells were treated with 10 μM CQ for 6 hours and then fixed. Autophagy-proficient (Ctrl) and -deficient (ATG7) HCT-116 CRISPR cells were treated with 10 μM CQ for 6 hours and then fixed. Cells were stained for total c-MET (green), LC3B (red) and nucleus (Hoechst dye-blue). Scale bar corresponds to 10 μm. (**b**) Representative immunofluorescence image showing total EGFR not colocalising with LC3B positive intracellular structures. Autophagy-proficient (shEGFP) HCT-116 *KRAS* WT cells were treated with 10 ng/ml Dox for 5 days. At day 5 of Dox treatment, cells were treated with 10 μM CQ for 6 hours and then fixed. Cells were stained for total EGFR (green), LC3B (red) and nucleus (Hoechst dye-blue). Scale bar corresponds to 10 μm. (**c**) Intracellular c-MET accumulation upon autophagy suppression. HCT-116 *KRAS* WT autophagy-proficient (shEGFP) and -compromised (shATG7 E8) cells were treated with 10 ng/ml Dox for 5 days. 6 hours prior to fixation cells were treated with 10 μM CQ. Cells were stained for total c-MET (green) and nucleus (Hoechst dye-blue). Bar plot depicts average intensity of intracellular c-MET/cell by using Fiji software (ImageJ). Quantification of intracellular c-MET was performed by manually specifying the intracellular region of interest (ROI) of every cell in a single z-stack image. Plasma membrane staining was excluded from quantification analysis. Bars represent mean ± s.e.m. of n= 40 shEGFP and n= 34 shATG7 E8 cells from three independent experiments. Images were acquired using a Zeiss LSM 700 confocal microscope. Post-acquisition brightness adjustments were identical between images of the same experiment and performed in Adobe Photoshop. White arrows show intracellular c-MET accumulation. Scale bar corresponds to 10 μm.

Figure 5 Genetic modulation of autophagy impairs mTORC2-mediated phosphorylation of AKT. Autophagy-proficient and -compromised HCT-116 and DLD-1 *KRAS* WT and G13D isogenic cell lines as well as CaCo2 cells were treated with Dox for 5 days and total cell lysates were subjected to immunoblot analysis for the indicated proteins. (**a-c**) ATG7 knockdown regulates AKT phosphorylation at S473 residue in CRC cells. Total cell lysates of autophagy-proficient (shEGFP) and -compromised (shATG7 E8) cells [(**a**) HCT-116, n=4; (**b**) DLD-1 n=3 and (**c**) CaCo2, n=4] were subjected to immunoblot analysis for ATG7, pAKT S473 and total AKT levels. β-actin was used as loading control. Bar plots represent densitometric analysis of pAKT S473 relative to total AKT. The bars represent mean ± standard deviation; ns= non-statistically significant, * $p<0.05$, ** $p<0.01$ and *** $p<0.001$. Two-way ANOVA statistical analysis was used for (**a**) and (**b**) and unpaired Student's t-test for (**c**). (**d-f**) Reduced AKT phosphorylation in autophagy-compromised cells does not regulate mTORC1 activation. Total cell lysates of autophagy-proficient (shEGFP) and -compromised (shATG7 E8) cells [(**d**) HCT-116 *KRAS* WT n=3 and *KRAS* G13D n=2; (**e**) DLD-1, n=2 and (**f**) CaCo2, n=3] were subjected to immunoblot analysis for ATG7, pS6 ribosomal protein S240/244 and total S6 ribosomal protein levels. Phosphorylation levels of S6 ribosomal protein depict activation level of

mTORC1. β-actin and total AKT were used as loading controls. Bar plots represent densitometric analysis of pS6 ribosomal protein relative to total S6 ribosomal protein or loading control. The bars represent mean ± standard deviation; ns= non-statistically significant. Unpaired Student's t-test statistical analysis was used for (**d**) and (**f**) cells. (**g-h**) HCT-116 CRISPR ATG7 knockout cells confirm pAKT S473 and mTORC1 findings observed by downregulation of ATG7. Total cell lysates of autophagy-proficient (Ctrl) and -deficient (ATG7) HCT-116 cells were subjected to immunoblot analysis for ATG7, pAKT S473 and pS6 ribosomal protein S240/244 relative to total AKT and total S6 ribosomal protein levels, respectively. Bar plots represent densitometric analysis of pAKT S473 relative to total AKT (**g**) and pS6 ribosomal protein relative to total S6 ribosomal protein (**h**). The bars represent mean ± standard deviation; ns= non-statistically significant, * $p<0.05$. Unpaired Student's t-test statistical analysis was used (n= 4).

Figure 6 Basal autophagy-mediated regulation of c-MET phosphorylation is linked with mTORC2 activation levels. (**a**) mTOR kinase inhibition in autophagy-proficient cells reduces phosphorylation levels of c-MET. Autophagy-proficient (shEGFP) and -compromised (shATG7 E8) HCT-116 *KRAS* WT cells were treated with 10 ng/ml Dox for 5 days. At day 5 of Dox treatment, cells were treated with 2 nM of the Torin 2 inhibitor for 6 hours and total cell lysates were subjected to immunoblotting for the indicated proteins. Bar plots represent densitometric quantification of p-c-MET Y1234/1235 relative to total c-MET protein and pAKT S473 relative to total AKT protein. The bars represent mean ± standard deviation of n=4; ns=non-significant; *** $p<0.001$. Two-way ANOVA statistical analysis was used. (**b**) Rapamycin treatment increases c-MET phosphorylation only in autophagy-proficient cells. Autophagy-proficient (Ctrl) and -deficient (ATG7) HCT-116 CRISPR cells were treated with 10 nM of Rapamycin for 3, 6 and 24 hours and total cell lysates were subjected to immunoblotting for the indicated proteins. Bar plots represent densitometric quantification of p-c-MET Y1234/1235 relative to total c-MET protein and pAKT S473 relative to total AKT protein (n=1).

Lampada et al. Figure 1

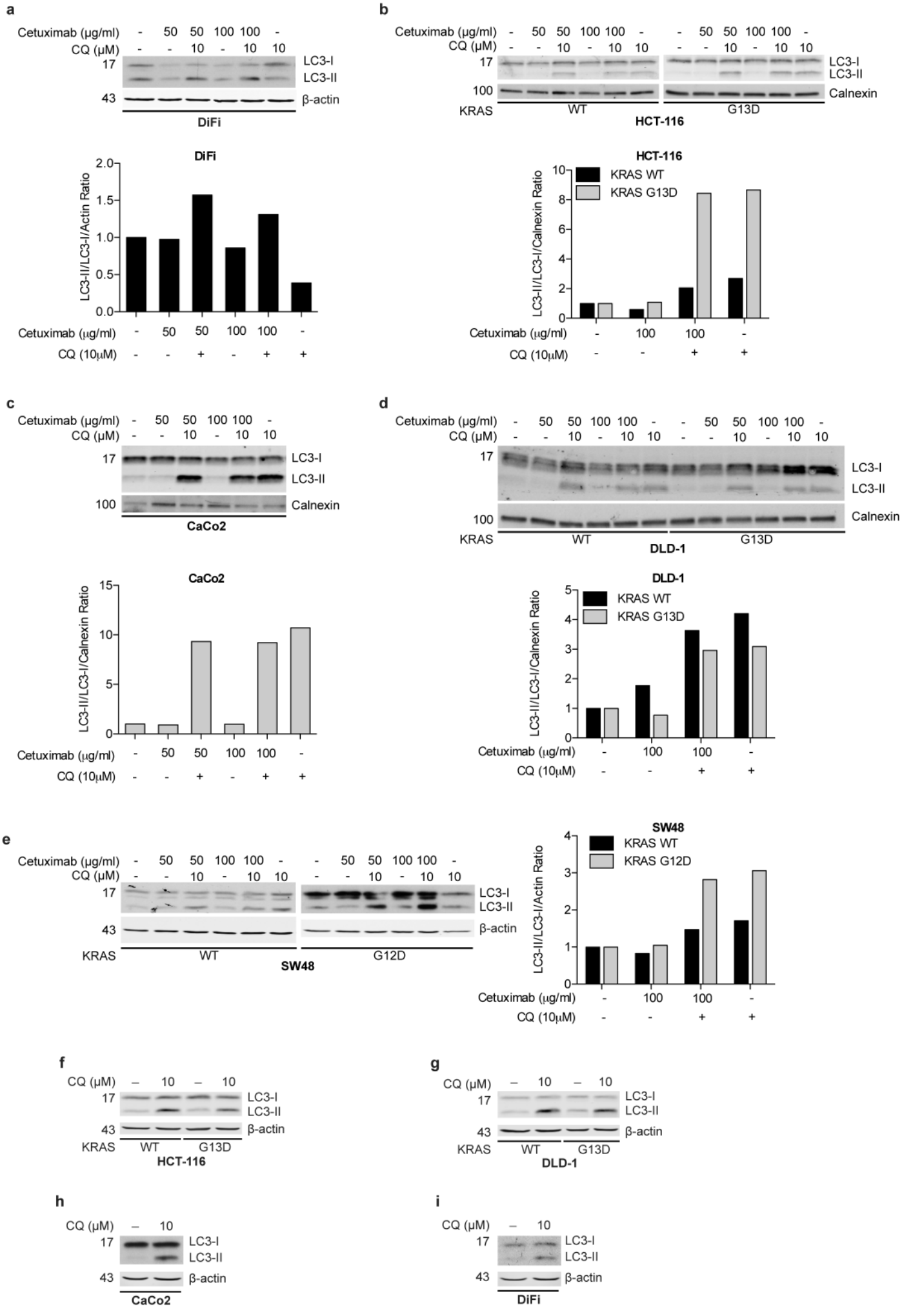

Lampada et al. Figure 2

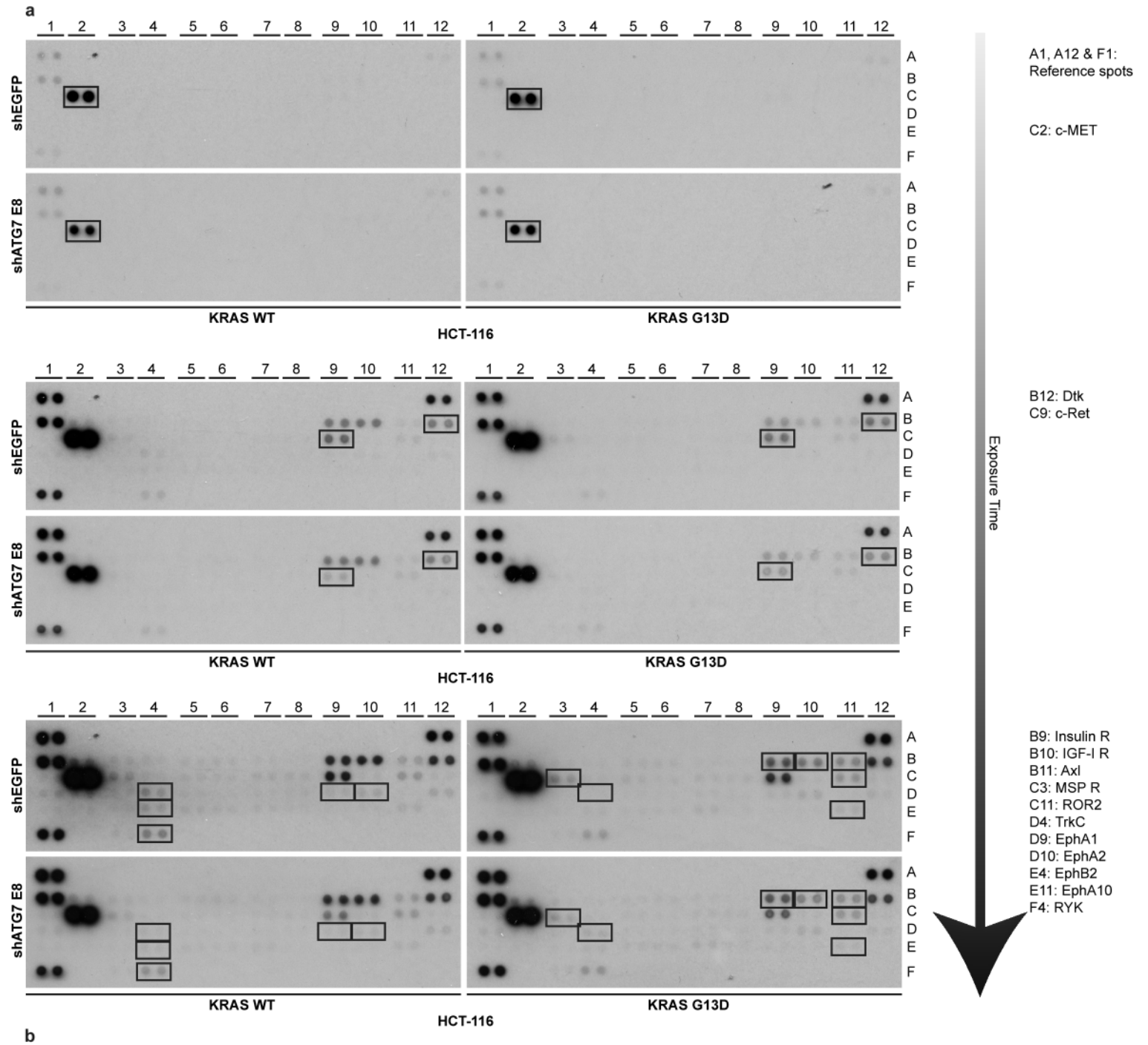

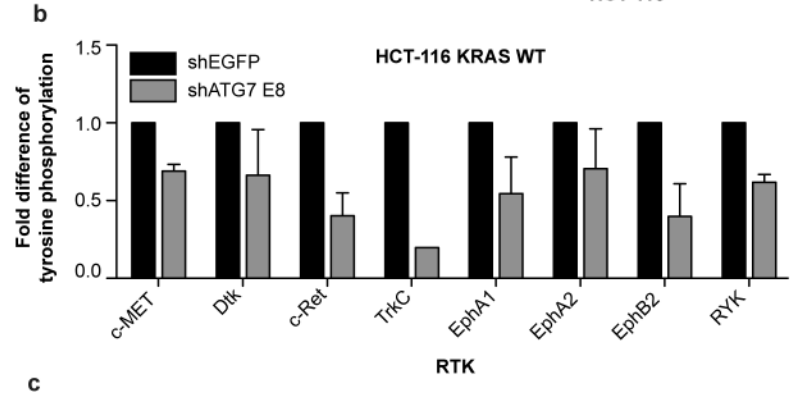

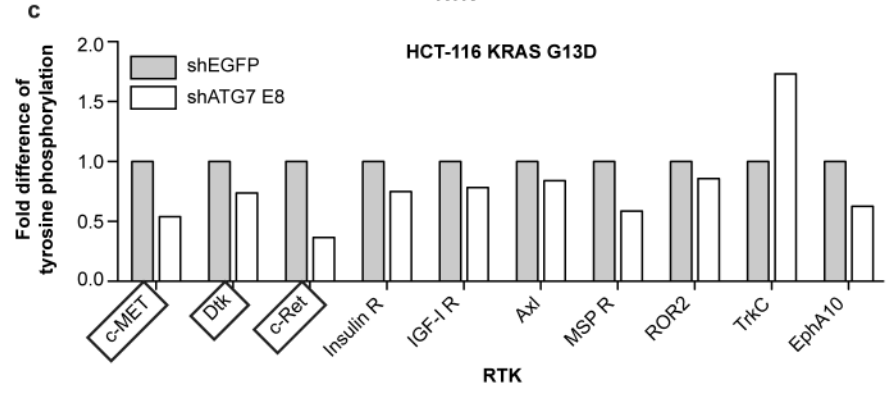

Lampada et al. Figure 3

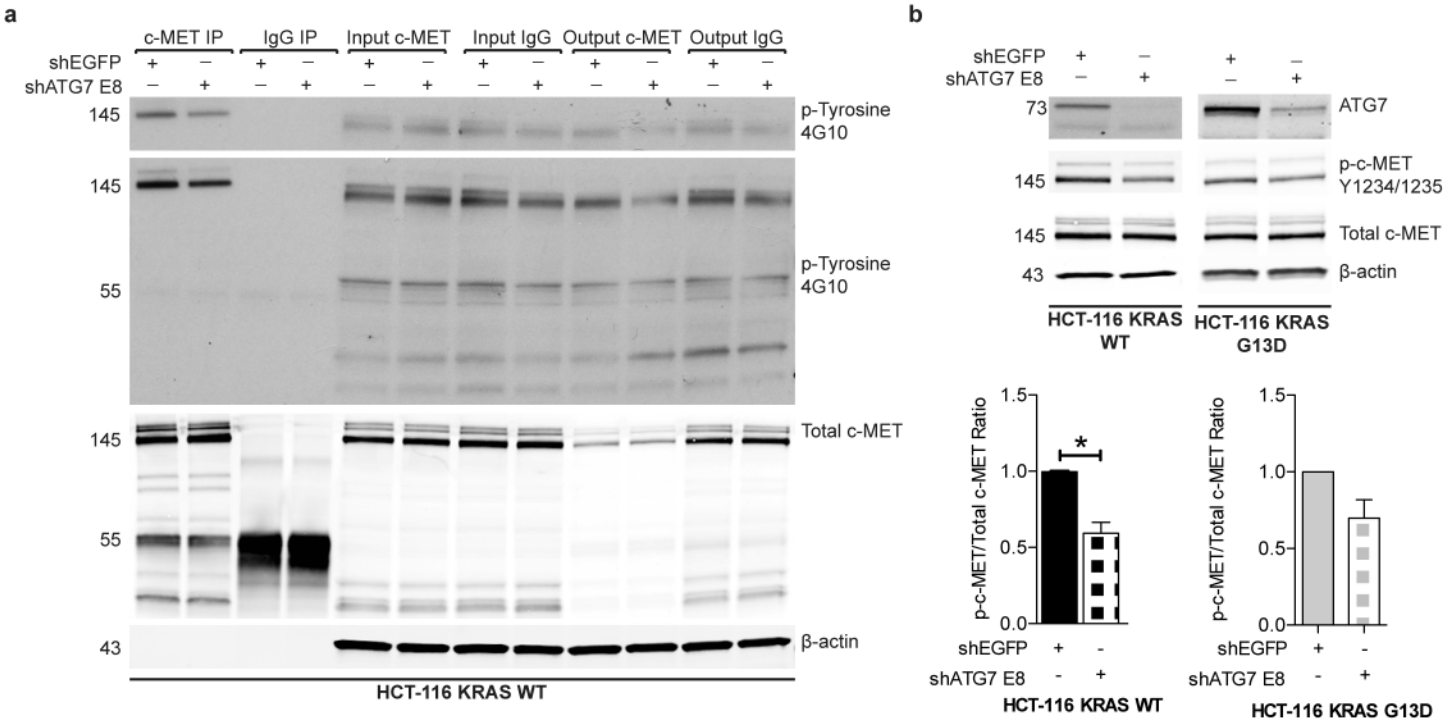

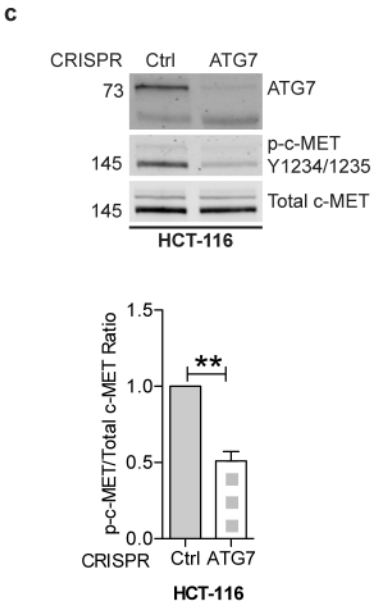

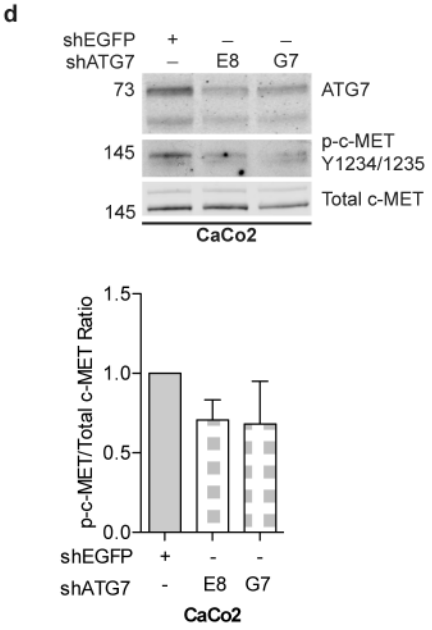

Lampada et al. Figure 4

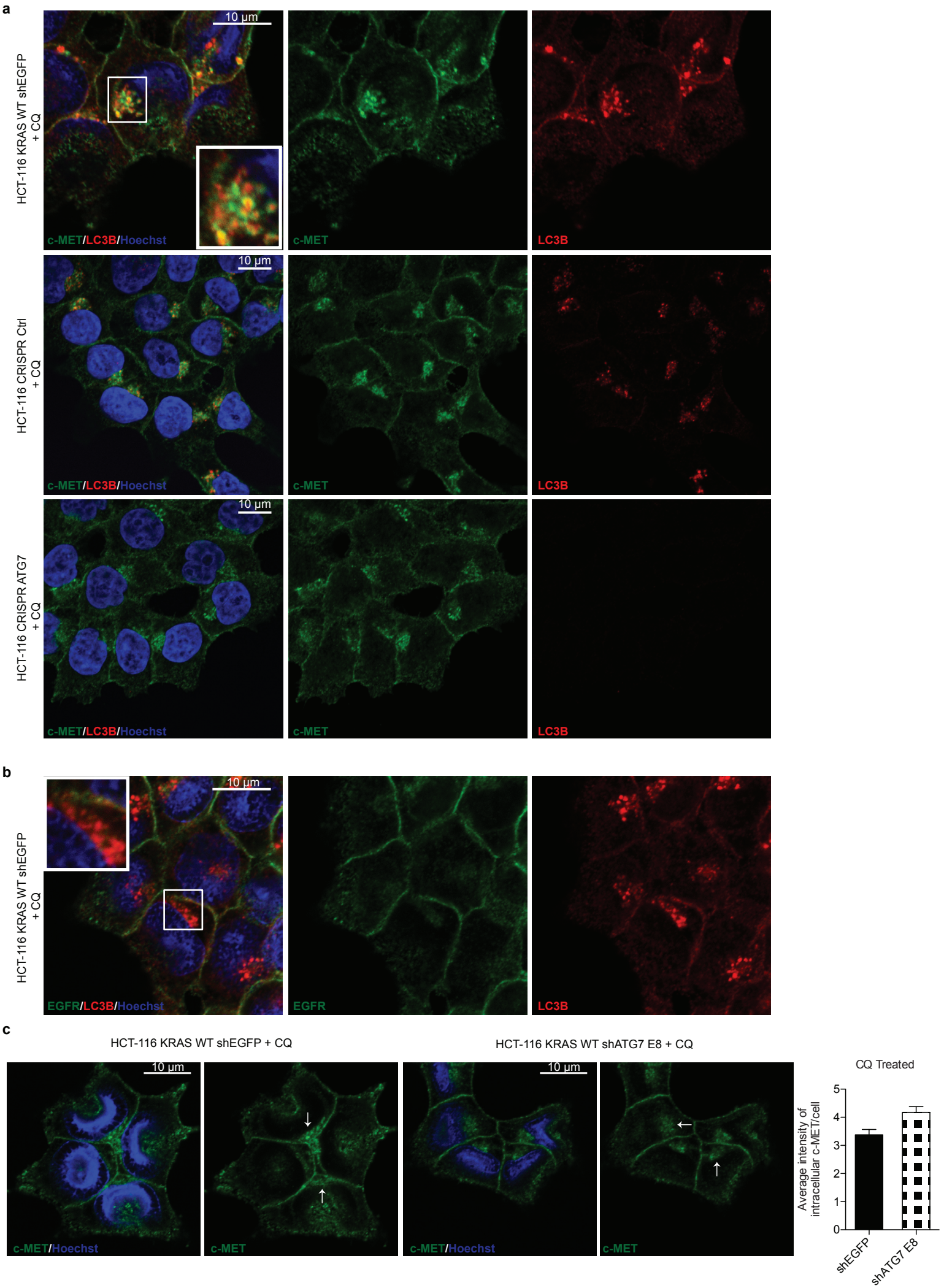

Lampada et al. Figure 5

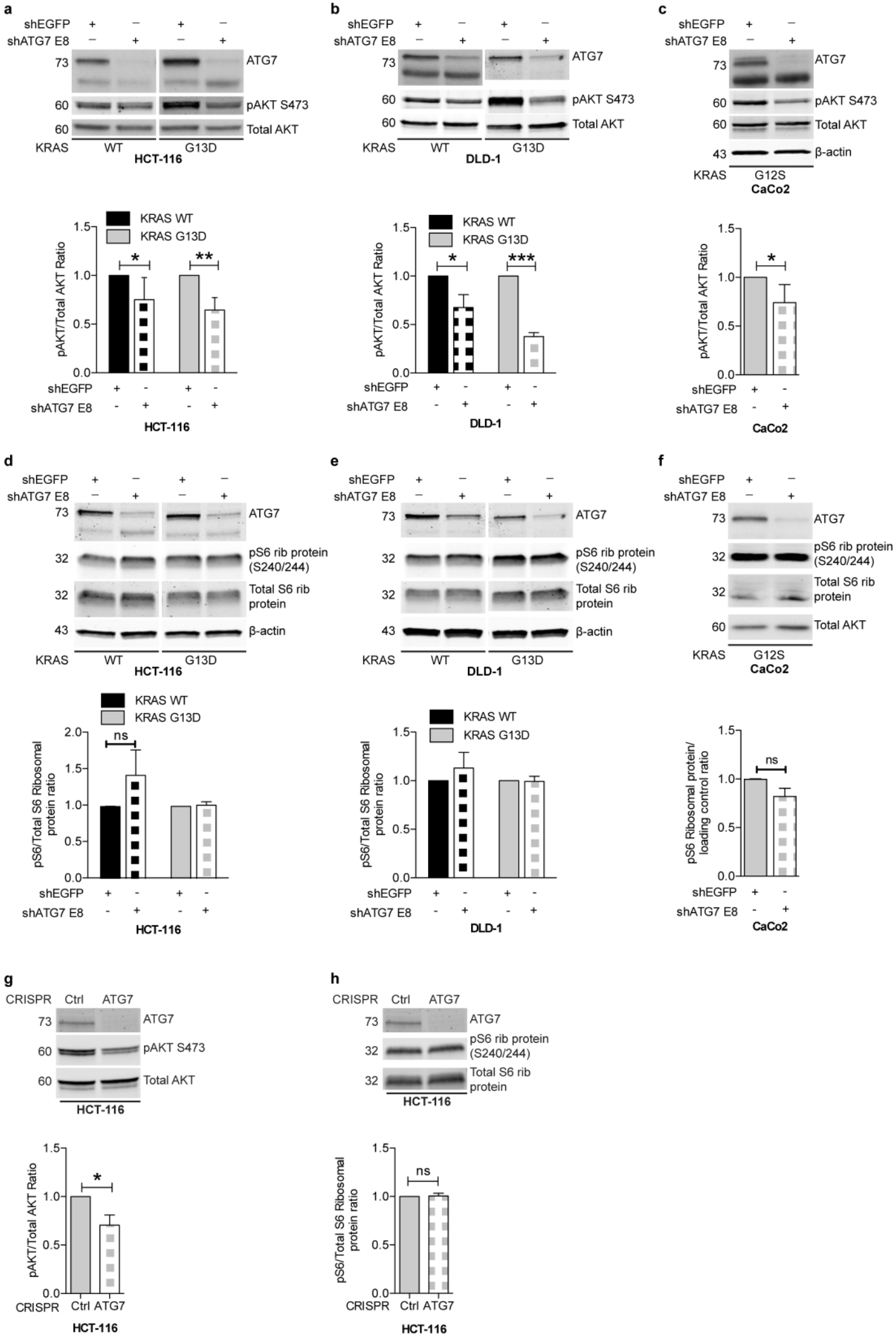

Lampada et al. Figure 6